Sediments in sea ice drive the Canada Basin surface Mn maximum: insights from an Arctic Mn ocean model

B. Rogalla[1], S. E. Allen[1], M. Colombo[1], P. G. Myers[2], K. J. Orians[1]

[1]Department of Earth, Ocean, and Atmospheric Sciences, University of British Columbia, Vancouver,

British Columbia V6T1Z4, Canada

[2]Department of Earth and Atmospheric Sciences, University of Alberta, 1-26 ESB, Edmonton, Alberta

T6G2E3, Canada

Key Points:

- We present an ocean model of Mn in the Canadian Arctic that captures observed spatial variation
- Non-local sediments transported by sea ice are a key source of micronutrients such as Mn to the Canada Basin
- Rivers are only important for Mn in coastal regions of the Canadian Arctic

Corresponding author: Birgit Rogalla, `brogalla@eoas.ubc.ca`

Abstract

Biogeochemical cycles in the Arctic Ocean are sensitive to the transport of materials from continental shelves into central basins by sea ice. However, it is difficult to assess the net effect of this supply mechanism due to the spatial heterogeneity of sea ice content. Manganese (Mn) is a micronutrient and tracer which integrates source fluctuations in space and time. The Arctic Ocean surface Mn maximum is attributed to freshwater, but studies struggle to distinguish sea ice and river contributions. Informed by observations from 2009 IPY and 2015 Canadian GEOTRACES cruises, we developed a three-dimensional dissolved Mn model within a 1/12 degree coupled ocean-ice model centered on the Canada Basin and the Canadian Arctic Archipelago (CAA). Simulations from 2002-2019 indicate that annually, 93% of Mn contributed to the Canada Basin upper ocean is released by sea ice, while rivers, although locally significant, contribute only 2%. Downstream, sea ice provides 34% of Mn transported from Parry Channel into Baffin Bay. While rivers are often considered the main source of Mn, our findings suggest that in the Canada Basin they are less important than sea ice. However, within the shelf-dominated CAA, both rivers and sediment resuspension are important. Climate induced disruption of the transpolar drift may reduce the Canada Basin Mn maximum and supply downstream. Other nutrient elements found in sediments, such as Fe, may be similarly affected. These results highlight the vulnerability of the biogeochemical supply mechanisms in the Arctic Ocean and the subpolar seas to climatic changes.

Plain Language Summary

Autumn storms on the Siberian side of the Arctic Ocean churn up sediment that freezes into sea ice. The prevailing ocean currents and winds push this sea ice across the Arctic Ocean towards the Canada Basin, where it melts and releases the sediment into the ocean. Sediment contains manganese (Mn) and other nutrient elements that help support plankton and life. Using our Mn ocean model, 93% of Mn in the Canada Basin comes from "dirty" sea ice from 2002 to 2019, while rivers supply 2%. As a result of climate change, less dirty sea ice may make it across the Arctic Ocean, which could reduce this supply system of Mn and other similar nutrients. This change also has potential impacts downstream: water from the Canada Basin travels through the shallow Canadian Arctic Archipelago (CAA) into Baffin Bay and eventually the North Atlantic. We found that about 34% of Mn transported along this route comes from "dirty" sea ice. In the CAA,

other sources contribute as well: tides churn up sediments from the ocean floor and many rivers flow into the channels. Our study highlights ways in which climate change may impact the nutrient supply systems in the Arctic Ocean.

1 Introduction

As the sea ice regime in the Arctic Ocean transitions from multi-year ice to predominantly first-year ice with overall reductions in sea ice extent, thickness and altered drift patterns (Stroeve et al., 2012; Stroeve & Notz, 2018; Spreen et al., 2011; Kwok et al., 2013), biogeochemical cycles and primary productivity are impacted through changes to the sea ice supply mechanism. The Arctic Ocean continental shelves connect land and ocean through the transfer of river runoff and sea ice from near-shore regions to the central basins (Charette et al., 2016). Reductions in sea ice export from the shelves weakens the long range transport of ice-rafted matter (Krumpen et al., 2019), including sediments (Dethleff et al., 2000; Darby et al., 2011), nutrients and trace metals (Tovar-Sánchez et al., 2010; Measures, 1999), pollutants (Pfirman et al., 1995; Peeken et al., 2018) and climate-relevant gases (Damm et al., 2018), to the surface ocean in regions far away from boundary sources. It is challenging to quantify the contribution of materials supplied by sea ice with observations alone due to the high spatial and temporal variability in the amount of sediment in sea ice and because it is difficult to distinguish it from additional contributions to the surface ocean such as river runoff. However, it is clear that changes to the physical processes in the Arctic Ocean will have impacts on the biogeochemical cycles and primary productivity of the basins themselves, as well as downstream in sub-polar seas (Drinkwater & Harding, 2001; Greene & Pershing, 2007).

Continental shelves cover half of the area of the Arctic Ocean (Jakobsson, 2002) and their shallow depths facilitate the incorporation of suspended matter into sea ice as it forms (Kempema et al., 1989). The narrow and deeper North American shelves are not as important for basin-wide sea ice sediment transport as the wide Siberian shelves (Eicken et al., 2005). In the Siberian shelf regions, fast ice builds up near shore in the fall, coinciding with storm-related resuspension events, forming sediment-rich sea ice (Nürnberg et al., 1994). The transpolar drift transports this sea ice towards the North Pole and the anticyclonic Beaufort Gyre redirects a portion into the Canada Basin. This passage takes several years, during which the ice undergoes cycles of melting, freezing and deformation. The materials released by melt alter the geochemical signature of the un-

derlying water (Pfirman et al., 1995). Several studies indicate an increase in sea ice exchange through increased drift speeds (Spreen et al., 2011; Kwok et al., 2013; Newton et al., 2017; Kipp et al., 2018), however a recent study indicates a disruption of the long range transport of sediments by sea ice due to the melt of first-year ice before it is incorporated into the transpolar drift (Krumpen et al., 2019) with implications for the surface ocean of the endmembers of this transport pathway: Fram Strait, and indirectly the Canada Basin, the Canadian Arctic Archipelago, and the subpolar North Atlantic. In order to establish the importance of sediment from sea ice for biogeochemical cycles in the indirectly impacted regions of the Canada Basin and the Canadian Arctic Archipelago, we developed a model of dissolved manganese (Mn).

Mn is a reactive trace element and an important micronutrient which shares many sources with iron (Fe) in the Arctic Ocean (Brand et al., 1983; Bruland et al., 1991; Jensen et al., 2020). Mn has a scavenged-type profile with high concentrations near sources and low background concentrations. This contrast makes it a convenient source tracer. Over the Arctic Ocean shelves, sediment resuspension contributes Mn to the lower water column (Evans & Nishioka, 2018; Colombo et al., 2020). However, the majority of external sources supply Mn to the ocean surface, contributing to the surface Mn maximum. In the Arctic Ocean, this surface maximum is attributed to freshwater sources (Campbell & Yeats, 1982; Yeats & Westerlund, 1991; Middag et al., 2011b; Cid et al., 2012; Kondo et al., 2016; Colombo et al., 2020). Observational studies have identified the origin of this freshwater as river discharge (Campbell & Yeats, 1982; Yeats & Westerlund, 1991; Evans & Nishioka, 2018), sea ice meltwater (Measures, 1999; S. Wang et al., 2014) (for Fe), or a combination of both (Middag et al., 2011b; Cid et al., 2012; Kondo et al., 2016; Colombo et al., 2020). Observations of riverine Mn indicate significantly higher concentrations than in the ocean (Colombo et al., 2019). Similarly, trace metals and nutrients in sea ice occur in concentrations in excess of those in the ocean (Campbell & Yeats, 1982; Hölemann et al., 1999; Granskog et al., 2003; Krachler et al., 2005; Aguilar-Islas et al., 2008; Tovar-Sánchez et al., 2010; Kondo et al., 2016; Evans & Nishioka, 2018). The importance of these components depends in part on the distance and pathway of input into the ocean (Fichot et al., 2013). So, while the Canada Basin is relatively distant from land, the narrow and shallow systems of channels that make up the CAA are in close contact with the land-ocean interface and may be more directly impacted by boundary processes such as river discharge and sedimentary inputs (Colombo et al., 2021).

In order to distinguish the individual importance of external Mn sources within the Canada Basin and the CAA, model studies are needed. Past studies have used tracers such as terrestrial dissolved organic matter (Fichot et al., 2013) and the oxygen isotope ratio (Yamamoto-Kawai et al., 2009) to distinguish the contributors to freshwater in the Canada Basin. Mn is an interesting complementary tracer because of its role as a nutrient and because it integrates processes that fluctuate on a short time scale. As a result, Mn helps address one of the main limitations of the study of sediment entrainment and export events by sea ice: that they are episodic and localized in nature (Eicken et al., 2005). Similarly, while sediment resuspension occurs intermittently, Mn integrates the effect of this component on the lower water column. After establishing the contributions of the Mn sources, we use Mn as a tool to study the general role of sea ice transport for biogeochemical cycles.

In this paper, we present a model of Mn in the Canadian Arctic Archipelago and the Canada Basin, informed by in situ observations collected during the 2009 IPY GEOTRACES cruise (Sim, 2018) and the 2015 Canadian GEOTRACES cruises (Colombo et al., 2020). Our work builds on the comprehensive first global model of Mn in the ocean (Van Hulten et al., 2017) and previous smaller scale models of Mn in the North Pacific Ocean (Johnson et al., 1996) and near hydrothermal vents (Lavelle et al., 1992). We incorporate new parameterizations for sediment resuspension, release of shelf sediments in sea ice, and fluvial contributions, to capture the drivers of Mn distributions in the Canadian Arctic. With this model, we show that the long range transport of sediments by sea ice from the Siberian shelves drives the surface Mn maximum in the Canada Basin while riverine contributions, although locally significant, are not as important as generally identified. Using these results, we discuss implications of future sea ice melt on Mn and Fe nutrient budgets in the Canada Basin and downstream in the Canadian Arctic Archipelago and Baffin Bay.
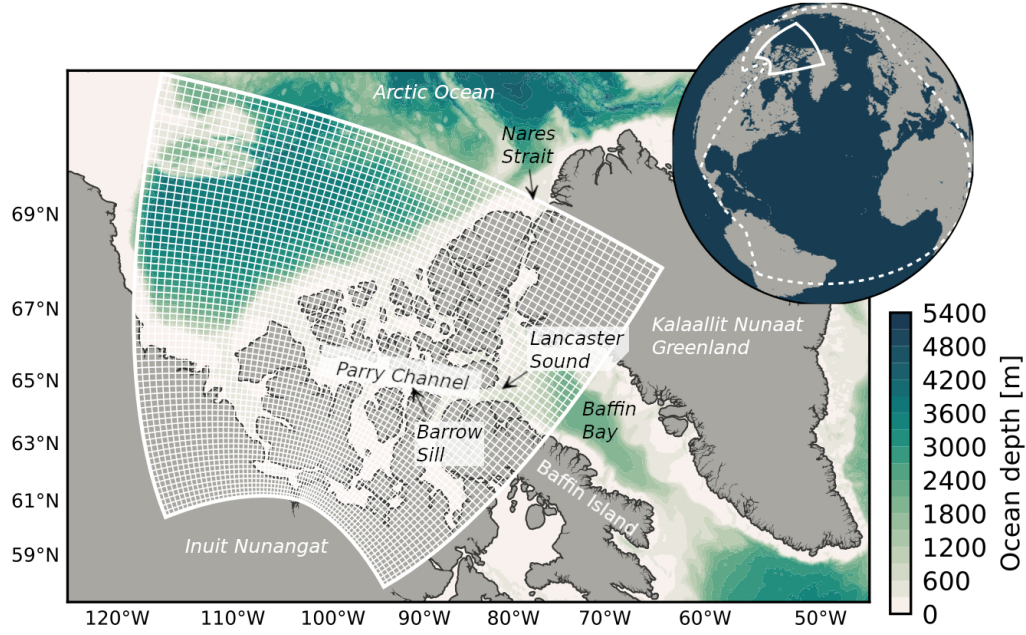
2 Methods

2.1 Coupled Ocean-Ice Model

For our simulations, we use ocean and ice dynamics calculated by the Arctic and Northern Hemispheric Atlantic (ANHA12) configuration (Hu et al., 2018) of the Nucleus for European Modelling of the Ocean (NEMO) version 3.4 (Madec, 2008). The ANHA12

143   configuration has a nominal horizontal resolution of 1/12° which resolves freshwater fluxes

144   associated with coastal currents in the CAA, as well as eddies (Bacon et al., 2014; Chel-

145   ton et al., 1998). The position of the grid's artificial pole in Northern Canada increases

146   the resolution in the CAA to about 2-3 km (Fig. 1). In the vertical, there are 50 depth

147   levels ranging from 1 m thickness at the surface to 454 m near the bottom. The bottom

148   bathymetry is represented using partial steps.

149   The ANHA12 domain has two open boundaries: one in Bering Strait and the other

150   at 20°S in the Atlantic Ocean. These boundaries are forced with Global Ocean Reanal-

151   yses and Simulations data (Masina et al., 2017). The ocean surface is forced with hourly

152   atmospheric data from the Canadian Meteorological Centre's global deterministic pre-

153   diction system (Smith et al., 2014) and the rivers are forced with monthly runoff clima-

154   tology with enhanced Greenland melt runoff (Dai et al., 2009; Bamber et al., 2012). The

155   river forcing from 2010 is repeated for the following years (Hu et al., 2019).

156   The sea ice in ANHA12 is represented using the dynamic and thermodynamic Louvain-

157   la-Neuve (LIM2) sea ice model with an elastic-viscous-plastic ice rheology (Fichefet &

158   Maqueda, 1997; Bouillon et al., 2009). An evaluation of LIM2 in the ANHA12 config-

159   uration is provided by Hu et al. (2018). The general spatial distribution of ice thickness

160   within the Archipelago is captured well. In the model, the northern CAA has very thick

161   sea ice (> 4 m), the central parts have intermediate thickness ice (2.5-3 m), and there

162   is thin (< 2 m) sea ice on the east side of the CAA and in southern channels. The ANHA12

163   simulations are limited by the lack of a land-fast ice parameterization, resulting in ice

164   velocities that are higher than observed in Parry Channel, impacting the winter trans-

165   port (Grivault et al., 2018). In addition, tides are not included and as a result, the polynyas

166   which form due to tidally enhanced mixing are not well reproduced (Hughes et al., 2018).

167   The advection and diffusion of tracers are calculated within NEMO by the TOP

168   engine (Gent et al., 1995; Lévy et al., 2001). Tracer advection is calculated with the To-

169   tal Variance Dissipation (TVD) scheme (Zalesak, 1979) and we use the Flow Relaxation

170   Scheme (FRS) for the tracer boundary conditions. The vertical diffusion of tracers is cal-

171   culated from the Turbulent Kinetic Energy closure scheme within ANHA12 and the hor-

172   izontal eddy diffusivity parameter is set to 50.0 m^2 s^{-1}.

Figure 1. The Mn model domain is centered on the Canadian Arctic Archipelago with highest horizontal resolution in the south (about 3 km). The nominal horizontal resolution of the grid is 1/12°; the white lines depict one in every ten grid points. The solid white line in the inset globe shows the Mn model domain extent, while the dashed white line delineates the domain of the Arctic and Northern Hemispheric Atlantic configuration (Hu et al., 2018) of the ocean-ice model.

2.2 Model of Mn in the Canadian Arctic

The Mn model runs offline in NEMO version 3.6 using five day averaged dynamics fields from the ANHA12 reference run from January 2002 to December 2019 (Hu et al., 2018). The Mn model consists of two main sets of computations: the advection and diffusion of tracers calculated by the NEMO-TOP engine (Gent et al., 1995; Lévy et al., 2001), and the source and sink contributions. The source and sink parameterizations were developed guided by observations from the 2015 Canadian GEOTRACES cruises (Colombo et al., 2020) and inspired by the first global model of Mn (Van Hulten et al., 2017). In order to reduce the computational cost, we calculate the model on a sub-domain of ANHA12, centered on the CAA (Fig. 1). Note that since we run offline, the physics originates from the full domain.

The known sources and sinks of Mn in the ocean are: rivers, hydrothermal vents, sediment diffusion, sediment resuspension, reversible scavenging, sinking, uptake and remineralization, atmospheric dust deposition, and flux from ice (Middag et al., 2011b; Balzer, 1982; Klinkhammer & Bender, 1980; Evans & Nishioka, 2018). From this list, we incorporate the processes that are important for dissolved Mn in the Arctic (summarized in Fig. 2 and Eqn. 1 and 2). In order to model the reversible scavenging of Mn, we incorporate Mn oxides (oMn) in addition to dissolved Mn (similar to Van Hulten et al. (2017); Eqn. 2). We do not model particle-bound Mn (pMn), but rather incorporate the indirect effect of pMn onto dMn through dissolution from the source components. We did not incorporate hydrothermal vents as a source of Mn in the Arctic, since the influence of the Gakkel Ridge is restricted to Nansen and Amundsen Basins due to scavenging nearby the source (Lavelle et al., 1992; Middag et al., 2011b). We also do not include sediment diffusion (reductive dissolution) because observations have indicated that these processes are not significant for Mn in the CAA (Colombo et al., 2020). The Mn model equations are:

$$\frac{\partial dMn}{\partial t} = S_{river} + S_{sediment} + S_{atm} + S_{ice} + S_{sed\ ice} + S_{bio} + R_{scav} + \text{advection} + \text{diffusion} \quad (1)$$

$$\frac{\partial oMn}{\partial t} = -R_{scav} - R_{sink} + \text{advection} + \text{diffusion} \quad (2)$$

which include the contribution of rivers, S_{river}, sediment resuspension (non-reductive dissolution), $S_{sediment}$, atmospheric dust deposition, S_{atm}, dust flux from ice, S_{ice}, sediment released by ice, $S_{sed\ ice}$, biological uptake and remineralization, S_{bio}, the reversible scavenging terms, R_{scav}, and sinking, R_{sink}. The details of the parameterizations are described in the following sections and the parameter values used for the runs are listed in Table 1.

The model was initialized with output from the global Mn model (Van Hulten et al., 2017) and concentrations are held constant at the sub-domain boundaries. At these boundaries, the ratio of dissolved to oxidised Mn from the global model were not representative (oxidised Mn was too low) and resulted in unusual scavenging behavior. To address this, we took values for the dissolved and oxidised Mn concentrations in a band 15 grid cells towards the interior of the basin (where the model had established normal scavenging behavior) from a test model run at the end of spin up and used those values for the boundary conditions.
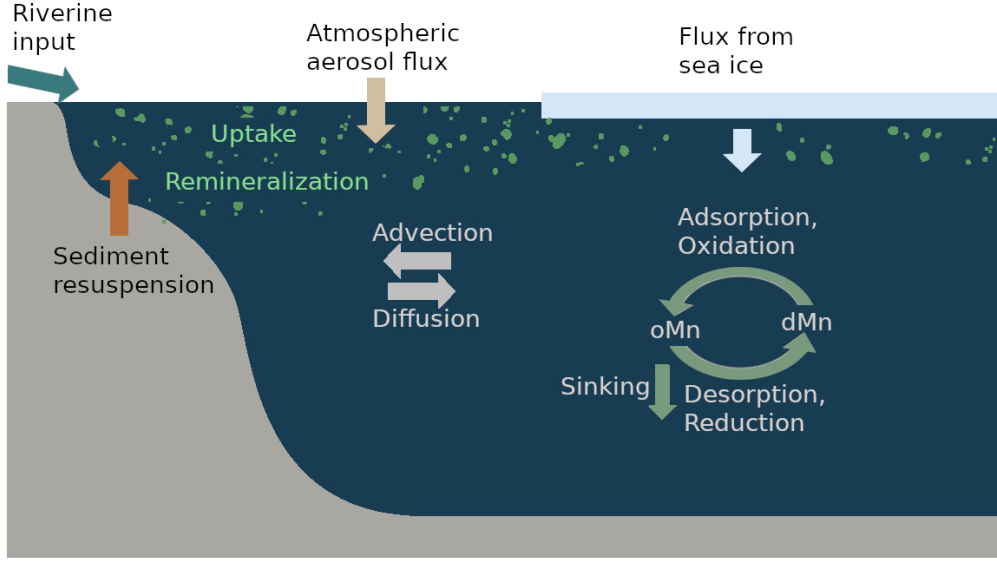
Table 1. Constants and parameter values used in the Mn model runs.

Parameter	Description	Value	Source
α_0	Solubility of Mn at 4°C	0.65	Fishwick et al. (2018)
$f_{Mn\ crust}$	Mn fraction in Earth's crust	527 ppm	Wedepohl (1995)
$f_{Mn\ sed}$	Mn fraction in marine sediment	270 ppm	Macdonald and Gobeil (2012)
m	Molar mass of Mn	54.938 g mol^{-1}	—
$R_{Mn:N}$	Extended Redfield ratio Mn:N	1.6 : 23,000	Kuss and Kremling (1999)
k_d	Reduction and desorption rate	$4.7 \cdot 10^{-7}$ s^{-1}	Bruland et al. (1994)
	Photo-enhanced reduction rate	$2.7 \cdot 10^{-5}$ s^{-1}	Sunda and Huntsman (1994)
k_p	Oxidation and adsorption rate	$7.0 \cdot 10^{-7}$ s^{-1}	This study[a]
s_{ox}	Sinking rate	0.6 m day^{-1}	Roy-Barman (2009) / This study
C	Tidal erosion tuning constant	$2.1 \cdot 10^{-6}$	This study
γ	Solubility tuning constant	0.065	This study
R / SPM	River characteristic content		This study[b]
	- Glacial	164 nM / 261 mg L^{-1}	
	- Continental	30 nM / 12 mg L^{-1}	
	- Other	2 nM / 4 mg L^{-1}	

[a]Using data from Colombo et al. (2020); Li (2017).

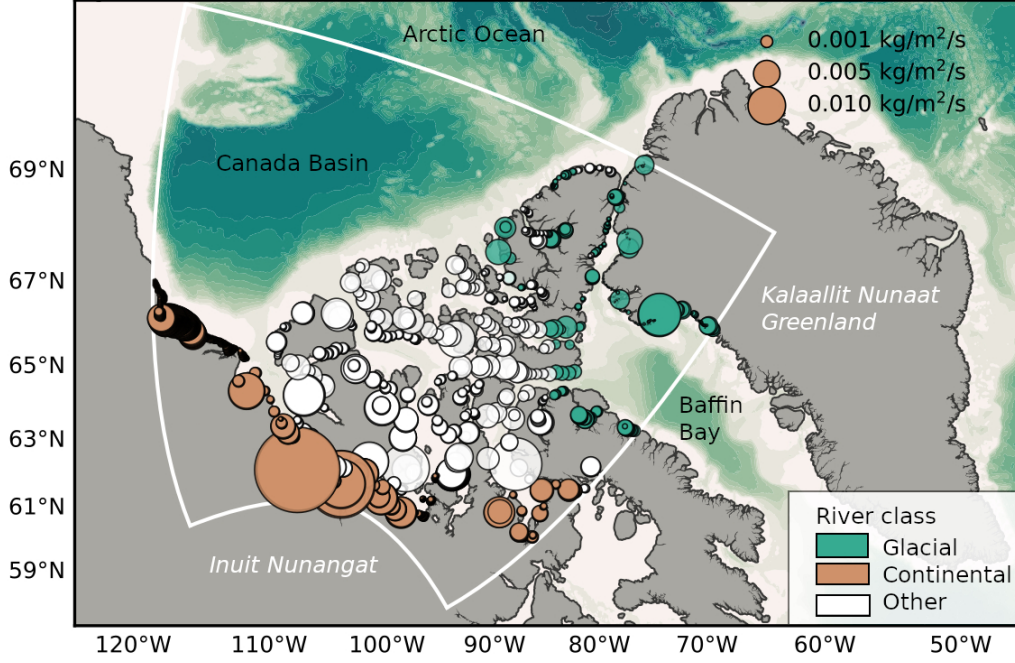[b]Using data from Colombo et al. (2019); Brown et al. (2020).

Figure 2. Summary of the processes that affect Mn concentrations in the Canadian Arctic Archipelago and the Canada Basin.

2.2.1 Riverine Source

River discharge contributes Mn to the shelf seas and into the Arctic Ocean (Middag et al., 2011a). Dissolved Mn is contributed directly in its dissolved form and indirectly through the dissolution from particle-bound Mn. The contribution of riverine Mn depends on the river discharge, Q, and the concentration in the rivers. These concentrations vary based on properties of the river's catchment basin: glacial rivers are strongly enriched in dissolved Mn, continental rivers are somewhat enriched, and in all other rivers, Mn is not significantly enriched (Colombo et al., 2019). At each time step, the rivers contribute dissolved Mn following:

$$S_{river} = \overbrace{\frac{Q}{\rho_0 \; \Delta z_{surface}} R_{class}}^{dissolved \; Mn} + \beta \; \overbrace{\frac{Q}{\rho_0 \; \Delta z_{surface}}}^{particle \; origin} \overbrace{\frac{SPM_{class} \cdot \alpha_0 \cdot f_{Mn, \; crust}}{m}}^{dissolved \; Mn} \tag{3}$$

where ρ_0 is the density of the river water, $\Delta z_{surface}$ is the surface grid box thickness, β is a factor which ranges from 0-1 in our experiments (not tuned, but tested in the upper bound river experiment), $f_{Mn, \; crust}$ is the crustal abundance of Mn, m is the molar mass of Mn, and α_0 is the solubility of Mn. We use an average value for the solubility (65%) measured in seawater at 4°C, since this lower temperature better reflects the

Figure 3. Model rivers were classified based on their drainage basin properties: glacial (green), continental (orange), or other (white). The points on this map are the locations of the river water input in the model and their sizes are proportional to the river discharge in September, 2015 (forcing is repeated from year 2010). Note that the river freshwater flux is remapped to prevent negative model salinities, hence some large rivers are represented as single point sources, while others such as the Mackenzie River consist of multiple point sources along the coastline (Hu et al., 2019).

CAA (Fishwick et al., 2018). This solubility falls within the range measured in samples across the world (Fishwick et al., 2018). Each river is assigned a class with an associated characteristic trace metal concentration, R_{class}, and suspended particulate matter content, SPM_{class}, based on catchment basin properties: glacial, continental, and other (Fig. 3 and Table 1). The Mn concentrations and SPM content associated with the classes are determined from rivers sampled in the CAA (Colombo et al., 2019; Brown et al., 2020).

2.2.2 Atmospheric Aerosol Flux and Release from Sea Ice

Atmospheric aerosols contribute Mn to the ocean through direct deposition to surface waters, Φ_{atm}, or through the deposition onto sea ice and the subsequent release dur-

237 ing melt, Φ_{ice}. We parameterized these contributions as:

$$S_{atm\ or\ ice} = \frac{\alpha_0 \cdot f_{Mn\ crust}}{m \cdot \Delta z_{surface}} \cdot \Phi_{atm\ or\ ice} \qquad (4)$$

238 The atmospheric and sea ice flux terms are derived from monthly Community Earth Sys-

239 tem Model (CESM) results. The combined monthly dry and wet atmospheric deposi-

240 tion fluxes originate from historical (1920-2005) and future (2006-2080) runs of the Com-

241 munity Atmosphere Model with Chemistry (CAM-Chem) downloaded from the Climate

242 Data Gateway (CESM1 CAM5 BGC Large Ensemble Atmosphere Post Processed Data;

243 Tilmes et al. (2016)). We estimate tracer fluxes from ice using the monthly Community

244 Ice CodE ensemble results (CICE; Holland et al. (2012); Kay et al. (2015)). These en-

245 semble run sets have a horizontal atmospheric resolution of 0.9 x 2.5° and ocean/ice res-

246 olution of 1.6 x 2.5° which we linearly interpolated to the ANHA12 grid. We do not tune

247 any of the parameters in this process.

2.2.3 Sediment Resuspension over the Continental Shelf

249 Dissolved Mn increases near the ocean floor in the Canadian Arctic as a result of

250 sediment resuspension (Colombo et al., 2020). Sediment resuspension occurs intermit-

251 tently, however, Mn integrates the resuspension events and thereby provides a cumula-

252 tive view of its prevalence. We incorporated sediment resuspension as a continuous pro-

253 cess:

$$S_{sediment} = \Phi_{erosion} \cdot \frac{\alpha \cdot f_{Mn\ sed}}{m \cdot \Delta z_{bottom}} \qquad (5)$$

254 where $f_{Mn\ sed}$ is the fraction of Mn in marine sediments. This fraction is likely to be lower

255 than measured in the continental crust, i.e. Wedepohl (1995), since it's undergone some

256 amount of chemical transformation. We used the Mn fraction estimated by Macdonald

257 and Gobeil (2012) from sediments in cores on the shelf and slopes surrounding the Canada

258 Basin. In Eqn. 5, $\Phi_{erosion}$ is the "erosion ability" (see Fig. S1 for the forcing field). This

259 term incorporates the spatial differences in dynamics within the CAA. West of Barrow

260 Sill, the system has lower mixing rates (Hughes et al., 2018) and tidal speeds (Epstein,

261 2018), than the region east of Barrow Sill and around the central sills area. These dif-

262 ferences impact the sediment resuspension rates, apparent in the much stronger near-

263 bottom increases of observed dMn in the eastern CAA (Colombo et al., 2020). We es-

264 timate the ability of sediment to be eroded with the barotropic tidal speed, U_{tidal}, and

a tuning constant, C:

$$\Phi_{erosion} = C \cdot U_{tidal}^2 \tag{6}$$

The barotropic tidal speeds are from the MOG2D-G model (Carrère & Lyard, 2003) and are significantly higher in the eastern CAA, compared to the western CAA (Epstein, 2018). Locations where the tidal speeds are less than 1 cm s^{-1} are masked, since they are below a critical threshold for motion for particles greater than 0.1 mm, i.e. sand. In areas where resuspension occurs frequently, the easily accessible Mn on particles has already been removed, resulting in a lower solubility. We reduce the solubility in Eqn. 5 at high tidal speeds according to:

$$\alpha = \alpha_0 \cdot \frac{\gamma(1 - e^{-U_{tidal}^2/\gamma})}{U_{tidal}^2} \tag{7}$$

where γ is a tuning parameter. At small tidal speeds, Eqn. 7 approaches α_0 while at tidal speeds greater than 0.1 m s^{-1}, solubility decreases and the overall resuspension rate approaches a constant $\alpha_0\gamma C$ (Fig. S2). The tuning parameters were estimated based on model behaviour in several tuning runs (see Section 2.3).

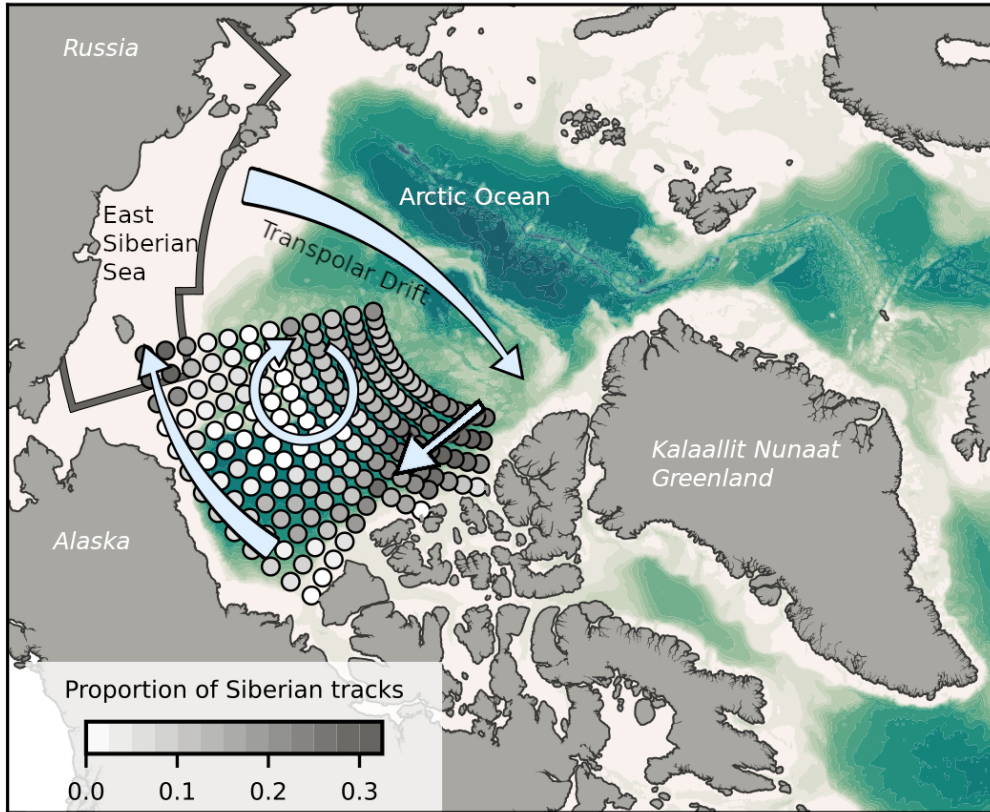### 2.2.4 Sediment Entrained in Sea Ice and Subsequent Melt

Sediment entrained in sea ice has been identified as an important source of reactive trace metals such as aluminum and iron in the ocean, and thus may also be important for Mn (Measures, 1999). In order to parameterize this contribution, we couple the Mn contained in sediments in sea ice and the sea ice melt rate, I_{melt}:

$$S_{sed\ ice} = \frac{\alpha_0 \cdot f_{Mn\ sed}}{m \cdot \Delta z_{surface}} \cdot S_p \cdot I_{melt} \tag{8}$$

where S_p is the sediment content in sea ice at each grid point. The sediment content is spatially variable, and depends on the amount of sediment that was incorporated during ice formation on the shelves and on sea ice transport.

Through particle tracking experiments with Ocean Parcels (Lange & Van Sebille, 2017), we estimated the contribution of sea ice formed over the Siberian shelves during the stormy fall months (September-December) to the ice in the Canada Basin (Fig. 4). We released parcels every month over the course of a year and traced them backwards for three years (the average sea ice age in the Canada Basin and the northwestern CAA based on satellite information). Almost 40% of the sea ice tracks in the northwestern CAA and Canada Basin region originated from the Siberian shelves via the transpolar drift

during the fall months, when strong sediment resuspension events coincide with sea ice formation. The results of the particle tracking experiments were interpolated and smoothed to create a forcing field which incorporates the spatial variation in sediment content in sea ice (Fig. S3). In addition, we assumed a low background value of shelf sediments in sea ice in the Archipelago. We multiply this forcing field by a tuned constant, 0.85 kg m^{-3}, which reflects the sediment content of the ice if it were fully formed over the Siberian shelf, i.e. the proportion of Siberian tracks was one.

Figure 4.   Sediment rich sea ice, produced over the Siberian shelves (East Siberian Sea; region definition outlined in brown) in the fall, is transported across the Arctic Ocean via the transpolar drift. From there it is found predominantly along the outer edges of the Beaufort Gyre; the largest contribution occurs in the northeastern CAA. Ice motion patterns are indicated with light blue arrows. For locations in the Canada Basin, the proportion of parcels traced back to the Siberian shelves (region defined with the brown outline) in the fall months are shown.

2.2.5 Uptake and Remineralization

Phytoplankton take up dissolved Mn in the euphotic zone and it is subsequently remineralized below the euphotic zone. We can quantify this contribution by pairing the addition and removal of Mn to the uptake and remineralization of nitrate:

$$S_{bio} = R_{Mn:N} \cdot \Delta N \tag{9}$$

where $R_{Mn:N}$ is the extended Redfield ratio for Mn to nitrogen based on observations in the North Atlantic (23,000 N : 1.6 Mn; Kuss and Kremling (1999)), and ΔN is the month-to-month change in nitrate concentration during the summer months (April-August) from 2002-2015 derived from the Canadian Ocean Ecosystem Model (CanOE; Hayashida et al. (2019)). We assume that the month-to-month change in nitrate is zero during seasons with low biological activity to avoid confusing the replenishment of nitrate via mixing with remineralization at the surface. We did not tune the uptake and remineralization.

2.2.6 Reversible Scavenging and Sinking

Dissolved Mn oxidizes forming larger aggregates and adsorbs to particle surfaces. dMn is regenerated by the reduction of oxidised Mn and desorption from particles. Since we do not directly model particle-bound Mn, but rather incorporate its effect on dMn through dissolution from the source components, we calculate the reversible scavenging based on the dissolved and oxidised Mn concentrations (Van Hulten et al., 2017):

$$R_{scav} = -k_p \cdot [dMn] + k_d \cdot [oMn] \tag{10}$$

where k_p is the adsorption and oxidation rate, and k_d is the desorption and reduction rate (see Text S1 for the full derivation). The R_{scav} term appears with opposing signs in the dMn and oMn equations (Eqn. 1 and 2). We estimate the rate constant k_p from observations of dissolved and particulate Mn in the Canadian Arctic (Li, 2017; Colombo et al., 2020). As this estimate is based on field data, the rate intrinsically incorporates the impact of abiotic and microbially enhanced oxidation. Assuming steady state, the ratio of the scavenging rates is equal to the ratio of dissolved to particulate Mn concentrations. This assumption reduces the available observations to those far away from sources and sinks, i.e. deep stations in Baffin Bay and the Canada Basin (Fig. S4). The ratio of scavenging rates, k_p/k_d, is estimated as 1.47 ± 0.25 and with a k_d of $4.7 \cdot 10^{-7}$ s^{-1}

(Bruland et al., 1994), k_p is estimated as $7.0 \cdot 10^{-7}$ s^{-1} (Fig. S5). The reduction rate, k_d, increases from the base rate up to $2.7 \cdot 10^{-5}$ s^{-1} in the euphotic zone (photo-enhanced reduction; Sunda and Huntsman (1994)), proportional to the solar flux that penetrates into the ocean at the surface (from ANHA12). We estimate the euphotic zone depth as 70 m in the Canada Basin with a gradual transition to 50 m in the CAA based on estimates by Bhatia et al. (2021) and Laney et al. (2017) (see Fig. S6). The scavenging rates in the model do not depend on the dissolved oxygen concentration since Arctic waters are generally well oxygenated.

The oxidised Mn aggregates sink, R_{sink}, and are removed through burial as in Van Hulten et al. (2017):

$$R_{sink} = s_{ox} \frac{\partial [oMn]}{\partial z} \tag{11}$$

where s_{ox} is the sinking rate. The sinking rate was based on the estimate by Roy-Barman (2009) of 0.4 m d^{-1} in the interior of the Arctic Ocean and then increased to 0.6 m d^{-1} based on an evaluation of modelled background oMn concentrations in the Canada Basin far away from sources and sinks.

2.3 Tuning

Of the parameters in our model (Table 1), we tuned the oMn sinking rate, sediment resuspension rate, sediment solubility parameter, and the sediment content in sea ice (in that order). Below, we describe our choice of criteria and approaches for tuning these parameters, and compare the parameter values with observations.

The sinking rate sets the background oMn (and through reduction, dMn) concentrations in regions far away from sources such as deep parts of the Canada Basin. We initialized the sinking rate in our model as 0.4 m d^{-1} based on a sinking rate derived by Roy-Barman (2009) from modelled and measured ^{230}Th profiles in the interior of the Arctic Ocean. With a sinking rate of 0.4 m d^{-1}, the deep oMn concentrations in the Canada Basin in the model were overestimated. An increased sinking rate of 0.6 m d^{-1} gave reasonable background oMn concentrations. The global model of Mn uses a sinking rate of 1 m d^{-1} up to 10 m d^{-1} to account for loss near hydrothermal vents (Van Hulten et al., 2017).

Our sediment resuspension parameterization incorporates two tuned parameters: the tidal erosion rate constant, C, and solubility parameter, γ. The tidal erosion rate

controls the background (below about 100 m) and near-bottom dMn concentrations in shelf areas, so in our domain predominantly the CAA. With observed dMn profiles in the CAA, we assessed the tidal erosion constant that best represented dMn in the lower water column with multiple test model runs. The solubility parameter limits the sediment resuspension rate in shelf regions with high tidal speeds, and the most appropriate value was estimated mainly based on comparing modelled dMn with observations at stations CAA6 and CAA9 (characterized by strong tidal speeds). The resultant sediment resuspension rates in our model range from 0 to 2808 g m^{-2} yr^{-1} (average is 95 g m^{-2} yr^{-1}). Particulate material collected in sediment traps over the Beaufort Shelf from spring 1987 to 1988 contained total dry weight particle fluxes ranging from 20 to 140 g m^{-2} yr^{-1} (O'Brien et al., 2006). The largest particle fluxes occurred during the summer and fall. Our average tuned sediment resuspension rate falls within this range.

We tuned the sediment content in sea ice last, as it is the most important parameter in our study. This parameter affects the surface dMn concentrations in regions where sea ice contains a significant proportion of non-local sediments (Fig. 4), so primarily the Canada Basin. We assessed the representation of surface dMn concentrations at stations in the Canada Basin after a few years of spin up using several values of the sediment content in ice parameter. The chosen sediment content in sea ice in the Canada Basin in our model ranges from 0 to 267 g m^{-3} (average is 64 g m^{-3}). In observations, the sediment load ranges by several orders of magnitude depending on the location sampled, the type of ice, and is highly variable year-to-year (see Table S1 for a non-comprehensive list of observed sediment content). In the Beaufort Sea, the observed sediment content in ice cores ranged from 31 to 593 g m^{-3} with an average of 157 g m^{-3} (Reimnitz et al., 1993). Our tuned ice sediment content is smaller, but of a similar order of magnitude.

2.4 Experimental Design

Three numerical experiments were performed with the Mn model, running from 2002 to 2019: the reference and "clean" sea ice cases, and a sensitivity experiment for the rivers. An additional experiment was performed from 2002 to 2015 to assess the magnitude of the impact of biological uptake and remineralization. The reference run includes all model components except uptake and remineralization, and uses a lower bound estimate of the river contributions (no particle-bound Mn, $\beta = 0$ in Eqn. 3). The clean

sea ice case is the same as the reference run, except that the sea ice does not contain sediment (i.e. $S_{sed\ ice} = 0$). In order to bound the riverine influence, we perform a sensitivity experiment with a distinctly upper bound riverine estimate ($\beta = 1$ in Eqn. 3), compared to the lower bound estimate from the reference run. The treatment of riverine Mn introduces uncertainties in the model due to the complex estuarine cycling and the influence of particulate matter on dissolved Mn concentrations. In the "upper bound" river experiment, we include the contribution from riverine sediments on the Mn concentrations in addition to the dissolved Mn.

Each experiment is spun up by repeating the year 2002 three times, before starting the full run. The run is considered spun up when the year-to-year change in Mn profiles is minimal (Fig. S7). Analysis was performed using Python 3 (https://anaconda.com) within Jupyter Notebooks with the NumPy, Pandas, SciPy, Matplotlib, Seaborn, scikit-learn, and cmocean packages (Pedregosa et al., 2011; Hunter, 2007; Kluyver et al., 2016; Oliphant, 2006; The Pandas development team, 2020; Thyng et al., 2016; Virtanen et al., 2020; Waskom & the Seaborn development team, 2020).
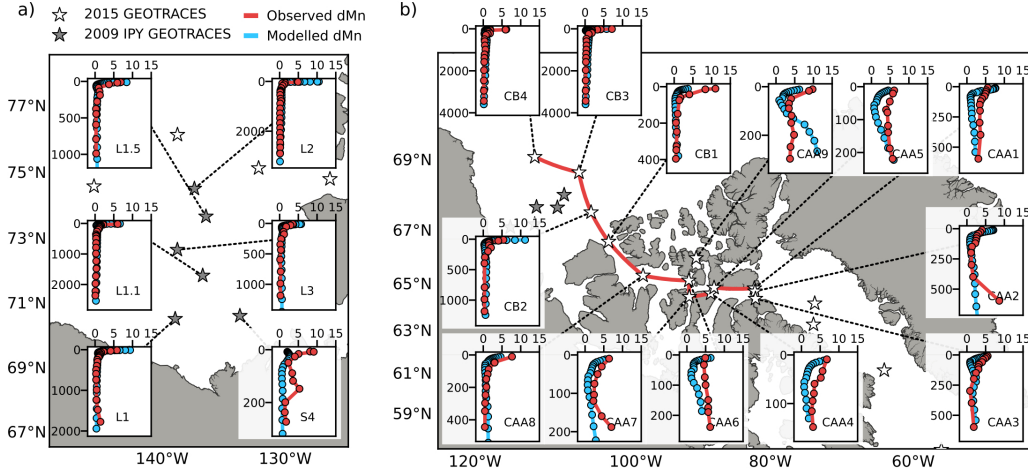
3 Results

Mn profiles throughout our domain are typical for a scavenged type element: concentrations are higher near sources with a low and homogeneous background (Fig. 5). The background concentrations are controlled by scavenging, sinking, advection and mixing, and the resultant redistribution of materials throughout the water column, while the surface Mn maximum is a result of the contributions from river runoff, sea ice melt, dust deposition, photoreduction, and sediment that is resuspended directly into the polar mixed layer. Sediment resuspension leads to near-bottom increases in some regions.

3.1 Model Evaluation

We evaluate the Mn model by comparing simulated dissolved Mn concentrations in August-September 2009 and 2015 from the reference experiment with measurements collected by the IPY and Canadian GEOTRACES cruises during those time periods (Sim (2018); Colombo et al. (2020); Fig. 5 and 6). We do not focus on particulate Mn as it is only incorporated into the model to improve the scavenging of dMn. Nevertheless, modelled oMn displays the observed variability in the upper 100 m in the CAA in 2015 well
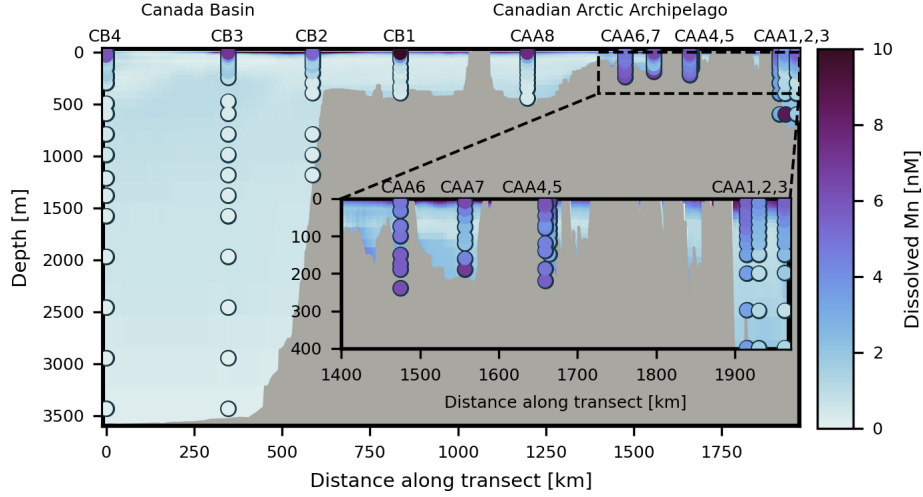
419 (Fig. S8). Overall, our intention is not to replicate the observations, but to incorporate

420 all the processes that control Mn distributions and to capture observed spatial variation.

421 The observations were not used in initial conditions or boundary conditions to allow for

422 an independent evaluation.

Figure 5. Simulated dissolved Mn profiles (blue) from the reference run compared to observed concentrations (red) from the (a) 2009 IPY GEOTRACES cruise on the Beaufort Shelf and (b) the 2015 Canadian GEOTRACES cruises in the Canadian Arctic Archipelago. Profiles are labelled with station names and their locations are marked with gray (2009 stations) and white (2015 stations) stars. Simulated concentrations were averaged over the time periods of the cruise observations, i.e. August-September. Note that the profile depth (vertical) scales vary.

423 The model captures the regional variation of Mn concentrations along a transect

424 from the deeper Canada Basin into the shallow CAA (Fig. 6). Observed surface concen-

425 trations range from 5-10 nM in the Canada Basin and on the Beaufort Shelf, up to 10-

426 11 nM at CB1, CAA8, and CAA9, and around 5 nM in the rest of the CAA (Fig. 5 and

427 6). The representation of the Canada Basin and the Beaufort shelf surface is variable

428 and dependent on the specific patterns of sea ice melt. Surface concentrations are over-

429 estimated at L2, L1, and CB2 and underestimated at S4 on the Beaufort shelf, and at

430 stations CB4, CB1, and CAA8 in the western CAA which receive outflow from the Canada

431 Basin. Within the CAA, surface concentrations are overestimated at stations CAA1 and

432 CAA2 in Lancaster Sound where waters from Baffin Bay recirculate, while on the south

433 side of the Channel at CAA3, the model captures the surface concentrations. Background

434 concentrations in the model and observations are low (0-2 nM) in the Canada Basin (0-

435 900 km along the transect in Fig. 6) and increase (to 1-4 nM) as the waters travel through

436 the shelf areas of the CAA.

Figure 6. A transect of Mn concentrations from the Canada Basin through Parry Channel in the Canadian Arctic Archipelago to Baffin Bay (path is shown in red in Fig. 5b). The background shading corresponds to simulated Mn averaged over the sampling time period (August-September, 2015) and the circles indicate observed Mn concentrations from the 2015 GEOTRACES cruises. The inset expands on the Parry Channel region east of Barrow Sill.

437   Within Parry Channel, background concentrations west of Barrow Sill are around

438 1-2 nM, similar to the Canada Basin, while in the eastern CAA they increase to 3-5 nM

439 with near-bottom maxima (appear as a slight bend in the modelled Mn profiles in Fig. 5

440 and Fig. 6). Background concentrations in shallow regions are set by the sediment re-

441 suspension rate which increases concentrations up to where the surface stratification lim-

442 its vertical mixing, while within the polar mixed layer concentrations are set by surface

443 sources. At depths of 40-100 m in the CAA, just below the polar mixed layer, the model

444 underestimates Mn. Within this depth range, Mn is remineralized, acting as a source

445 that is not considered in the reference experiment. In the biological experiment, we es-

446 timate that remineralization accounts for up to 0.3 nM (Fig. S15 and Text S3). At 100-

447 200 m depth in the Canada Basin and on the Beaufort shelf, observed Mn concentra-

448 tions are slightly higher than the background concentrations. This increase is associated

with the winter Bering Sea Water and is not captured by the model, as it was not represented in the model's western boundary condition.
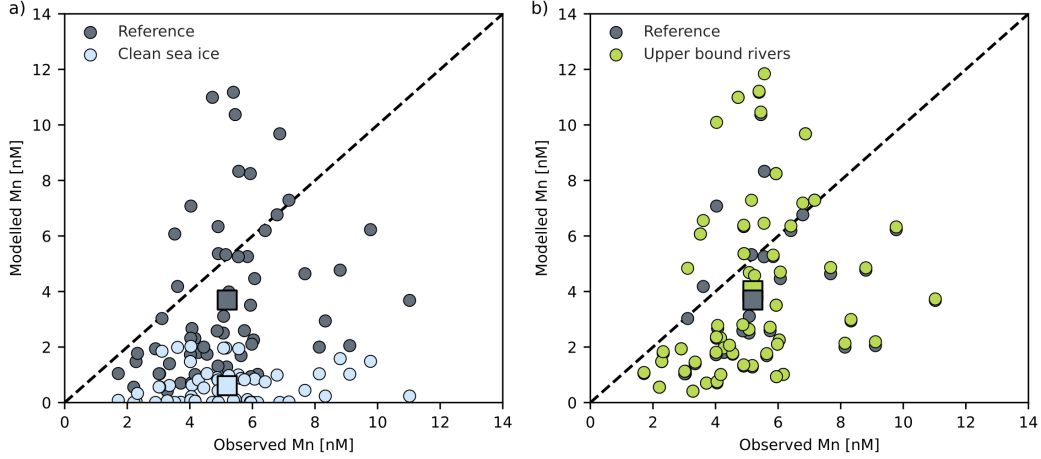
The net effect of sediment resuspension is well-represented in the background concentrations, however there are a couple of unusual modelled near-bottom Mn profiles (Fig. 5). At station CAA9 in Penny Strait, the Mn model overestimates background and bottom concentrations by 5 nM. At this station, strong mixing results in constant, "vertical" observed Mn profiles (Hughes et al., 2018). Sediment resuspension, based on tidal stress, dominates as a source of Mn to this region. However, this version of the physical model does not incorporate tides. Hence, we add Mn at the bottom, proportional to the strength of tidal stress, without redistributing it due to tidal mixing. At stations CAA2 and CAA7, on the south side of Parry Channel, observed Mn concentrations increase up to 10 nM near the ocean bottom. These peaks in the observations are attributed to sediment resuspension (Colombo et al., 2020), although the specific mechanism for the strong peak is unclear. The model does not reproduce these local extreme increases, which likely vary on much smaller spatial scales than our parameterizations can resolve. An increase in Mn over the 40 m above the bottom is reproduced by the model at stations CAA2, CAA4, CAA5 and CAA7.

While the model is limited in its representation of regions with strongly variable resuspension rates, it performs well within a range of environments: from deep regions in the Canada Basin to shallow areas in the CAA. The model is configured to ask questions about the drivers of Mn variability; it is important to keep in mind that our parameterizations are limited by the spatial and temporal resolution of available information, so small scale variations are unlikely to be captured by the model.

3.2 Importance of Sediment in Sea Ice

In order to evaluate the importance of sea ice and rivers on the representation of Mn in the upper water column (above 50 m), we compare the results of the "clean" sea ice and upper bound river experiments with the reference experiment (Fig. 7). For all experiments, the representation of surface concentrations has a broad spread. The "clean" sea ice experiment underestimates concentrations in the upper water column by several nM (Fig. 7a) and its mean underestimates concentrations by 4 nM. The mean of the reference run, with sediment in sea ice, falls within 1 nM of observed concentrations. The

upper bound river experiment slightly increases the surface concentrations relative to

the reference experiment, particularly in the eastern CAA (Fig. 7b). Estimates for sta-

tions in the Canada Basin are unaffected by the addition of particulate matter in rivers.

Figure 7. Nearest-depth modelled Mn concentrations compared with observations for depths shallower than 50 m for all stations (2009 and 2015). Square markers indicate the averages of the experiments and observations. (a) The modelled Mn concentrations at the evaluation stations most closely resemble the observations in the reference experiment with sediment in sea ice compared to the "clean" sea ice experiment. Both of these experiments use the lower bound river estimate. (b) The lower and upper bound river experiments, which include sediment within the sea ice, indicate that additional contribution from riverine particulate matter has a relatively small impact.

We expect substantial vertical gradients in concentrations in the surface layer in

the Arctic Ocean as a result of the strong stratification. The shallowest observations are

collected at around 10 m below the surface, while the shallowest model estimate is at

0.5 m depth, so it is difficult to assess the uppermost modelled concentrations. However,

the Mn-salinity relationship in the model is similar to the observations for the experi-

ment with sediment in sea ice (Fig. S9). In the "clean" sea ice experiment, the model

significantly underestimates the low-salinity Mn endmember.

3.3 Contributions from External Sources of Mn

To assess the relative contributions of each of the external Mn sources, we calculated the annual contribution and flux from these model components in the reference experiment. We are most interested in the surface layer, so our estimate is for the upper 55 m of the water column. An estimate of the full water column differs by including the effects of resuspension in regions deeper than 55 m, thus increasing the importance of resuspension (Table S2). Estimates from the upper bound river experiment, which does not account for any removal of particulate or dissolved Mn in estuaries, are indicated in brackets. We did not include the contributions from (photo)reduction and remineralization as sources of dMn in these calculations since they are part of the internal cycling of Mn. In order to identify regional differences, we separated the domain into the Canada Basin and the Canadian Arctic Archipelago (details in Fig. S10) and subdivided the CAA into west and east along 100°W. Overall, the Canada Basin is more isolated and receives a lower annual contribution of Mn than the CAA: 238 (254) versus 370 (530) μmol m^{-2} yr^{-1} (Table 2).

In our model, the dominant source of Mn in the Canada Basin is the release of sediment by sea ice melt (Table 2); it accounts for 93 (87)% of the average yearly addition of Mn. The amount of melt fluctuates interannually, similar to sea ice area changes observed with satellite data. Nevertheless, from 2002 to 2019, sea ice melt is consistently the largest contributor of Mn in our model in the Canada Basin. Sediment resuspension contributes about 4.7 (4.4)% in the Canada Basin, mainly over the Beaufort shelf, and river discharge, predominantly from the Mackenzie River, contributes 2.2 (8.5)%. Atmospheric dust deposited onto the ocean surface, or released during sea ice melt, is not a significant source of Mn anywhere in the domain.

In the CAA, sediment resuspension contributes 58 (40)% of the annual external addition of Mn to the water column (Table 2). Sediment released by sea ice accounts for 37 (26)% of Mn; a combination of relatively "clean" sea ice with high melt rates. The river contributions cover a broader range from 5.0-34% in the CAA, compared to 2.2-8.5% in the Canada Basin. Since the total annual Mn addition is greater in the CAA, rivers contribute significantly more dMn to the CAA. Although the Canada Basin receives runoff from the Mackenzie River, the CAA has many rivers of a range of sizes that drain into it, including glacial rivers with high characteristic Mn concentrations.

Table 2. The spatial average annual dissolved Mn contributed by external model source components to the upper 55 m of the water column (μmol m^{-2} yr^{-1}) in the reference experiment, averaged over the years 2002-2019, separated by region (Fig. S10). Sediment release by sea ice is the only component that varies significantly year-to-year. Estimates from the upper bound river experiment are indicated in brackets.

	Canada Basin		Canadian Arctic Archipelago	
Component contribution	μmol m^{-2} yr^{-1}	%	μmol m^{-2} yr^{-1}	%
River discharge	5.3 (22)	2.2 (8.5)	19 (178)	5.0 (34)
Sediment resuspension	11	4.7 (4.4)	213	58 (40)
Sediment from sea ice	221	93 (87)	138	37 (26)
Dust released by sea ice	0.2	0.1	0.3	0.1
Direct dust deposition	0.0	0.0	0.0	0.0
Total	238 (254)	100	370 (530)	100

Table 3. Same as Table 2, but with the Canadian Arctic Archipelago (CAA) subdivided into western and eastern halves along 100°W (near Barrow Sill).

	Western CAA		Eastern CAA	
Component contribution	μmol m^{-2} yr^{-1}	%	μmol m^{-2} yr^{-1}	%
River discharge	6.5 (28)	2.2 (8.7)	27 (289)	6.5 (42)
Sediment resuspension	155	52 (49)	256	61 (37)
Sediment from sea ice	136	46 (43)	140	33 (20)
Dust released by sea ice	0.3	0.1	0.3	0.1
Direct dust deposition	0.0	0.0	0.0	0.0
Total	297 (318)	100	424 (686)	100

Within the CAA, there is a significant difference in dynamical regime west and east of the approximately 120 m deep Barrow Sill (Table 3; Hughes et al. (2017); Colombo et al. (2020, 2021); Q. Wang et al. (2012)). The overall contribution of Mn to the water column in the eastern CAA is 424 (686) μmol m^{-2} yr^{-1}, compared to 297 (318) μmol m^{-2} yr^{-1} in the west. The main contributor to this difference is the 1.6 times stronger sediment resuspension in the eastern CAA. In addition, rivers contribute more strongly to the east-
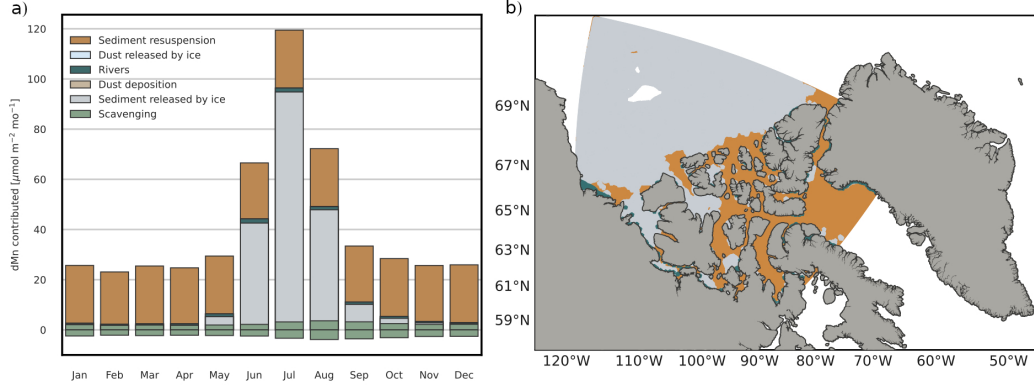
ern CAA relative to the western CAA, 6.5 (42)% versus 2.2 (8.7)%, with a broader range in the estimate of their role in the eastern CAA. The eastern CAA receives contributions from the high Mn content glacial rivers that drain Greenland, Ellesmere Island, and Baffin Island.

Throughout our domain, Mn concentrations are highest in the summer months as a result of seasonally fluctuating components (Fig. 8a). Sea ice melt is largest in July, while the river runoff peak occurs during the freshet in May-June. Due to the large supply of dissolved Mn in the summer months and the increased solar flux, (photo)reduction and oxidation are stronger from July through September. For the month of September, we identified which component on average controls Mn for each horizontal grid cell over the full time series (Fig. 8b). Note that this figure shows where the model adds the contribution from a component; where the Mn ends up depends on the advection and diffusion of the tracer as well.

Within the Canada Basin and portions of the western CAA (the Amundsen Gulf and western Parry Channel), sea ice melt controls the simulated Mn concentrations (Fig. 8b). In the interior of the Beaufort Gyre region, far away from sources and with relatively "clean" sea ice, none of the components contribute significantly. Over the Beaufort Shelf, the Mackenzie River is a regionally important source of Mn; generally river runoff is a significant source at river mouths. In the shallower shelf regions, such as the Beaufort Shelf and the CAA, sediment resuspension is prevalent.

The magnitudes of annual Mn fluxes from sources in this Arctic Model (AM; Table 2) are comparable to those in the first global model of Mn by Van Hulten et al. (2017) (VH). In the global model, dust contributes 0-2 μmol m^{-2} yr^{-1} in the Arctic Ocean, whereas in AM it ranged from 0-0.3 μmol m^{-2} yr^{-1} (combining direct dust deposition from the atmosphere and indirect release from ice). AM riverine fluxes were 5.3 (22) μmol m^{-2} yr^{-1} in the Canada Basin and 19 (178) μmol m^{-2} yr^{-1} in the CAA; higher than the VH estimate of 0-2 μmol m^{-2} yr^{-1}. This range likely reflects a combination of the high Mn content of rivers in the Arctic (Colombo et al., 2019) and alternate treatment of rivers; VH assumes a relation between Fe and Mn content, while AM uses observations specific to the Arctic rivers and their catchment basins. In the global model, the flux of Mn from bottom sediments in the Arctic Ocean was 5-75 μmol m^{-2} yr^{-1}; AM has 11-213 μmol m^{-2} yr^{-1}. The difference in the upper limit of the range likely reflects the distinctive processes con-

Figure 8. Sediment released by sea ice dominates Mn contributions in the Canada Basin and peaks in July, while sediment resuspension is prevalent over shelf areas including the Canadian Arctic Archipelago. (a) Climatology of the seasonal cycle of Mn contributions for the full water column. The oxidation (removal) and reduction (addition) of Mn through scavenging are calculated as the average through the water column. Sediment resuspension is added at the bottom grid cell, while all other sources act directly on the ocean surface. The contributions from dust deposition and release from ice are too small to appear. (b) Most important Mn contributors to the water column in September based on climatology. At each grid cell, the color represents the most important model forcing component. The importance of scavenging is based on the average combined effect of reduction and oxidation throughout the water column. Places within the model domain where the net contributions are smaller than 0.5 μmol m^{-2} mo^{-1} are white (i.e. in the Canada Basin).

sidered by the models: the global model considers sediment diffusion for the flux from sediments, whereas AM considers sediment resuspension because it is more important in the CAA (Colombo et al., 2020). It is also challenging to resolve the large continental shelf regions in the Canadian Arctic in a global model. Lastly, on a global scale, hydrothermal input of Mn at spreading ridges is important (Van Hulten et al., 2017), however the spreading ridges in the Arctic are far away from the AM domain, so that contribution is not included.

3.4 Simulated Surficial Mn During the Summer and the Polar Night

The most significant seasonal and interannual changes in Mn concentrations occur in the polar mixed layer, defined here as the upper 35 m of the water column. For the following characterizations of the simulated concentrations, we will focus on this layer. The upper few meters of the ocean have a strong gradient in Mn concentrations (simulated profile in Fig. S11). It is not possible to measure this layer with conventional methods from a large ship. As such, we exclude the surface 3 m in the results presented here (see Fig. S12 for the surface Mn field) to allow for more direct comparison with existing observations.
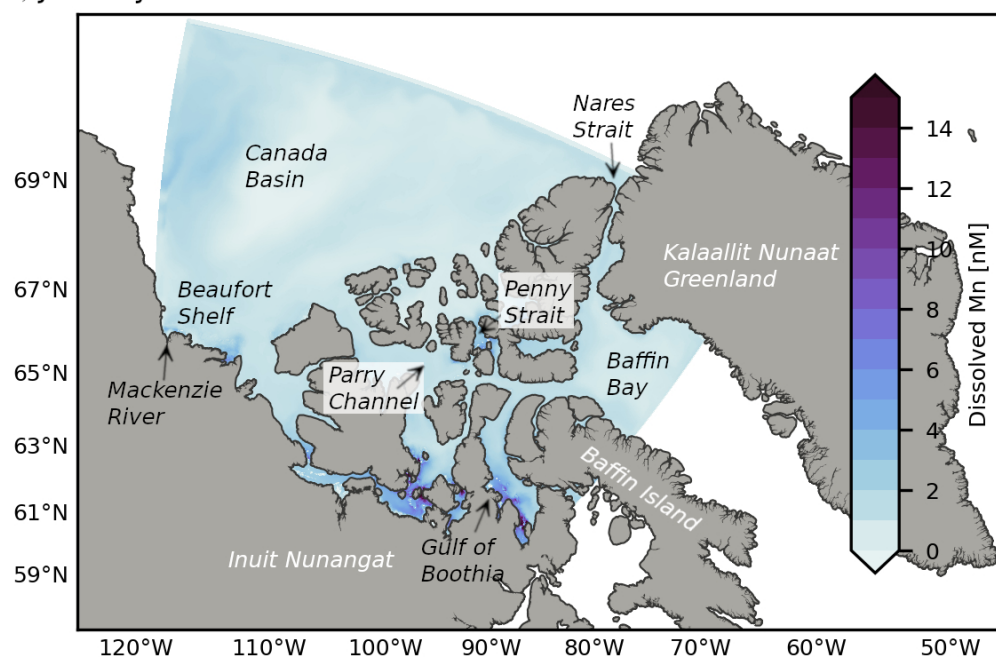
During summer months, the surface Mn concentrations in the Canada Basin mirror the areas of strong sea ice melt (Fig. 9a). The highest Mn values are found along the outer edges of the Beaufort Gyre (up to 14 nM). Although rivers contribute only a few percent annually to Mn in the Canada Basin (Table 2), over the continental shelf, plumes of higher Mn concentrations extend along coastlines in the summer, starting during the spring freshet (Fig. 9a and Fig. 8b). The plume from the Mackenzie River, the largest river in our domain, extends eastward along the shelf in August, 2015. Glacial drainage is apparent in surface Mn concentrations in a number of coastal regions (Fig. 9a). Along the coast of Greenland, high concentration Mn runoff drains the ice sheet and a number of plumes are visible extending from Nares Strait. In the northern CAA, higher surface concentrations result from a combination of sea ice melt and glacial runoff (Fig. 8b).

Mn concentrations exhibit spatial variability within the CAA (Fig. 9). In west-central CAA, concentrations are low (2-6 nM) and homogeneous. Southern regions, including the Gulf of Boothia, have some of the highest concentrations (8-14+ nM) and flow into the Parry Channel east of Barrow Sill. In this section of central and eastern Parry Chan-

Figure 9. Simulated monthly Mn concentrations in the Polar Mixed Layer, excluding the surface three meters to allow for direct comparison with observations (surface fields in Fig. S12). (a) August, 2015. In the summer, sea ice melt and sediment resuspension dominate the Mn concentrations in the Canada Basin and the Canadian Arctic Archipelago, while freshwater sources such as the Mackenzie River and Greenland meltwater are important regionally. (b) January, 2015. During the Polar night, simulated Mn concentrations are homogeneous and low, however sediment resuspension continues to drive higher concentrations in south-central CAA.

nel (and Penny Strait), intermediate concentrations (4-8 nM) are present. In Lancaster Sound, the outflow from Parry Channel follows the southern half of the channel while waters from Baffin Bay (5-8 nM) recirculate along the northern half of Lancaster Sound. Baffin Bay is characterized by lower interior surface concentrations and higher bands associated with Nares Strait and Lancaster Sound outflow.

During the Polar Night, fewer sources contribute Mn (Fig. 8a) and there is less spatial contrast in surface concentrations (Fig. 9b). Surface concentrations range from 1-5 nM (excluding the Gulf of Boothia region), while in the summer they ranged up to 14 nM. Scavenging has removed the relic of summer surface source signatures. Regions where Mn is most impacted by sediment resuspension (Fig. 8b), such as the Gulf of Boothia, still have high concentrations in the winter as this component does not vary seasonally.

4 Discussion

In the Arctic Ocean, maximum Mn concentrations occur near the surface in the polar mixed layer. These high concentrations are commonly attributed to freshwater sources such as river discharge and sea ice melt (Campbell & Yeats, 1982; Yeats & Westerlund, 1991; Middag et al., 2011b; Cid et al., 2012; Kondo et al., 2016; Colombo et al., 2020). However, the relative contributions from rivers and sea ice to this low-salinity maximum are not easily distinguished. In this paper, we present a regional model of Mn in the Canadian Arctic which incorporates river input and sediment release by sea ice, as well as atmospheric inputs, sediment resuspension, uptake and remineralization, scavenging, and sinking. With these components, the model captures the spatial variability and magnitude of observed concentrations and we are able to use the model to assess the controls on Mn in the Arctic. With results from three Mn model experiments (reference, "clean" sea ice, and upper bound river), we identified the dominance of non-local sediment released by sea ice in the Canada Basin, while rivers had a more regional importance. These findings suggest that future changes to sea ice transport across the Arctic Ocean may have a significant impact on the supply of Mn and other micronutrients to the Canada Basin and downstream to the CAA. Within the CAA, the dynamical differences between the western and eastern CAA translated into distinctive mean Mn concentrations and component contribution patterns with more influence from rivers and sediment resuspension.

4.1 Ice-rafted Sediments are the Predominant Source of Mn in the Canada Basin

With our model, we found that 93 (87)% of Mn in the Canada Basin (the main estimate is from the reference experiment with the upper bound river estimate in brackets) is supplied by sediment from sea ice and 37 (26)% in the CAA (Table 2). Sediments released by sea ice melt dominate the Mn concentrations in the polar mixed layer during the summer months (Fig. 9a), while in the winter, sea ice blocks the direct surface input of Mn and a lower, more homogeneous distribution results (Fig. 9b). Sediment transport and release by sea ice is the main source of Mn (and likely other similar nutrients) within the Canada Basin, and plays a role within the CAA as well. The sea ice in the interior of the Canada Basin originates from the Siberian shelf regions and traverses the Arctic Ocean via the transpolar drift. It spends several years in transit, during which it undergoes freeze-thaw cycles and loses some sediment. In our parameterization, the highest Mn concentrations (and relatively younger ice) are found along the outer edges of the Beaufort Gyre in the Canada Basin, while older ice transported to the interior of the Gyre by convergence has lower Mn concentrations (Fig. 9a). Sea ice formed over the Beaufort Shelf is transported towards Siberia and does not directly impact the Mn concentrations in the Canada Basin.

Mn sources from the land-ocean interface, such as rivers and sediments, were more important in the CAA than in the Canada Basin, and dynamical differences between the western and eastern CAA translated into distinctive Mn concentrations and component contribution patterns. This separation in dynamics is bounded by the ≈120 m deep Barrow Sill and has been noted in several studies (Hughes et al., 2017; Colombo et al., 2020). In the western CAA, surface concentrations range from 2-6 nM (Fig. 9) and Mn component contributions share characteristics with the Canada Basin: similar overall river contributions, significant influence from sediments in sea ice, and weaker contributions from sediment resuspension (Table 3). In contrast, in the eastern CAA, Mn concentrations are higher (4-8 nM; Fig. 9) and dominated by sediment resuspension associated with strong tidal speeds and river discharge play a more important role. The estimate of the component contributions is most sensitive in the eastern CAA: the importance of rivers ranges from 6.5% to 42% depending on the treatment of particulate matter. Rivers are prevalent in the eastern CAA and many of these drain glaciated regions associated with high suspended particulate matter and dissolved Mn. As a result, rivers have the poten-

tial to play an important role in the eastern CAA. However, the available information for river input and estuarine removal, limits our ability to constrain the most likely river contribution. Based on the surface concentration comparisons (Fig. 7), the upper bound river experiment alters the mean representation slightly; it is inconclusive on the most realistic representation. The uncertainties associated with these estimates highlight the need for studies looking at the estuarine cycling in the CAA.

Besides sea ice melt, Pacific water inflow from the Bering Strait and river runoff (Eurasian runoff and North American runoff) contribute freshwater to the Arctic Ocean (Proshutinsky et al., 2019; Krishfield et al., 2014) and could contribute Mn to the surface maximum. The central Canada Basin contains significant amounts of meteoric water and sea ice melt (Guay et al., 2009) which feed its freshening (Yamamoto-Kawai et al., 2009). Several studies have looked into the composition of this water. Fichot et al. (2013) did not identify much river runoff in the central basin and Kelly et al. (2019) found that the freshwater contribution from Siberian rivers has decreased since 1997 as a result of the mainly anticyclonic atmospheric circulation pattern over the Canada Basin. Similarly, model trajectories of floats released from Siberian rivers since 1985 do not generally reach the Canada Basin by 2007 (Proshutinsky et al., 2019). In our reference and upper bound river simulations, rivers contribute only 2.2 (8.5)% to the total budget of Mn in the Canada Basin and 5.0 (34)% in the CAA (Table 2). However, freshwater sources such as the Mackenzie River on the Beaufort shelf and glacial melt off the coast of Greenland (Fig. 9a) can dominate areas nearby coastlines. The supply of relatively fresh Pacific Water from Bering Strait to the Canada Basin is also affected by the atmospheric circulation in the Canada Basin (Kelly et al., 2019) and floats released from Bering Strait since 2000 do not enter the central Canada Basin by 2012 (Proshutinsky et al., 2019). Thus, inputs outside of our domain that originate from Siberian runoff and Pacific water are unlikely to significantly contribute to the freshwater-associated surface Mn maximum in the Canada Basin. It is important to note that our simulated profiles (Fig. 5) do not capture the subtle increase in Mn concentrations associated with the winter Bering Sea Water around 100-200 m depth in the Canada Basin and on the Beaufort Shelf. This limitation is likely because our western boundary condition does not fully capture the higher concentrations of Mn found in the Alaskan Coastal Current and in waters from the Chukchi Shelf.

In order to assess whether we overestimated the sediment content of sea ice, we performed an experiment with "clean" sea ice. In the "clean" ice experiment, the surface Mn concentrations are underestimated by 4 nmol L^{-1} relative to observations (Fig. 7a). If we assume that all of the missing Mn comes from sediment and that Mn added at the surface mixes down to the turbocline, we miss a source that supplies 13-213 grams of sediment per squared meter to the surface ocean across the Canada Basin (range based on model turbocline depths in 2015). The magnitude of this component is similar to the average sediment load measured in sea ice cores (Reimnitz et al., 1993; Stierle & Eicken, 2002; Eicken et al., 2005). Rivers would be unable to contribute the total amount missing since it must occur over a large area and since the upper bound river experiment shows that additional contributions from rivers do not significantly affect the Canada Basin or the overall surface representation (Fig. 7b, Table 2). In the "clean" sea ice experiment, the freshwater endmember of Mn is also underestimated (Fig. S9). The Mn-salinity relationship in the Canada Basin and the CAA is more accurately represented in the experiment with sediment contained in sea ice and the regional differences are also reproduced.

Our results demonstrate that the long range transport of sediments by sea ice from the Siberian shelves is an important source of Mn in the Canada Basin and the Canadian Arctic Archipelago. These findings provide support for the sea ice trace metal transport mechanism proposed by Measures (1999). Measures (1999) found that the highest Al and Fe concentrations in the central Arctic Ocean coincided with areas with high concentrations of ice-rafted sediments, instead of river input, and so they hypothesized that transport of ice rafted sediments and the subsequent seasonal melt supplies reactive elements to the surface Arctic Ocean. However, their data set did not allow the quantification of annual fluxes of material to the central Arctic Ocean and so they were unable to quantify the exact contribution of this component to the observed trace metal concentrations.

4.2 Declining Long Range Sea Ice Transport Could Reduce the Canada Basin and Canadian Arctic Archipelago Nutrient Supply

Based on the importance of non-local sediments transported by sea ice (particularly from the Siberian shelves), the distributions of trace metals, nutrients, and their biogeochemical cycles in the Arctic basins are likely to be significantly impacted by cli-
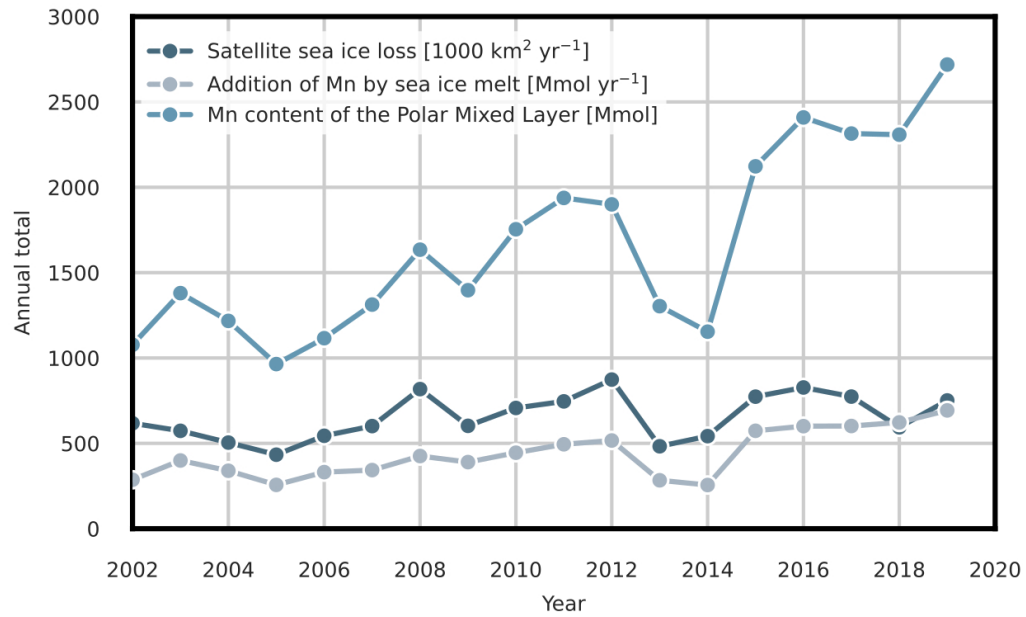
mate change associated reductions in sea ice. Rising oceanic and atmospheric temperatures delay the freeze-up period and induce earlier melt of sea ice (Stroeve et al., 2012; Stroeve & Notz, 2018). In addition, in the relatively "quiet" dynamics of the Arctic Ocean, increased mixing may bring warmer Atlantic water (or Pacific Water; Kodaira et al. (2020)) to the surface and further increase sea ice melt (D'Asaro & Morison, 1992; Liang & Losch, 2018). These factors may significantly reduce the amount of first-year ice that survives in the Kara Sea, East Siberian sea, and western Laptev Sea (Krumpen et al., 2019).

Studies of the transpolar ice drift indicate an increase in drift speed associated with a thinning ice cover and as a result, an increase in exchange of ice-rafted material between regions (Spreen et al., 2011; Kwok et al., 2013; Newton et al., 2017; Kipp et al., 2018). However, in recent years, summer ice extents have been small enough in the marginal ice zones, that most of the ice exported from shelves melts before it enters the transpolar drift (Krumpen et al., 2019). These findings suggest a reduction in the transport of matter towards the central Arctic Ocean and Fram Strait by the transpolar ice drift.

In our study, we saw a steady increase in the Mn content of the Canada Basin polar mixed layer from 2002-2019 (Fig. 10), and the primary source of this Mn is sea ice melt (correlation R-squared of 0.96). Note that our experiments do not account for interannual changes in sea ice supply regions. The addition of Mn by melt in our model mirrors satellite observations of sea ice loss in the Beaufort Sea (Fig. 10; correlation R-squared of 0.54). Whereas in the short term, there may be an increase in nutrients supplied by sea ice into the Canada Basin through increased sea ice exchange and melt volume, in the long run, we expect a decrease in supply of sediment rich sea ice from the Siberian shelves via the transpolar drift and a subsequent decline in the surface maximum of Mn in the Canada Basin. Confounding this is the likely increase in transport of riverine and shelf-derived trace elements in the ocean by the transpolar drift as a result of an intensification of the Arctic hydrological cycle and permafrost degradation (Charette et al., 2020).

A reduction in micronutrient supply to the Canada Basin may also have an impact downstream in Baffin Bay. With our experiments, we calculated the transport of Mn through Parry Channel and the contribution of sediment released by sea ice melt to this transport (see Text S2 for details). About 87% of the net Mn transported into Parry Channel from the Canada Basin is contributed by sediments from sea ice (Fig. S13 and S14).

Figure 10. Interannual variations in sea ice melt contribute strongly to Mn supply to the Canada Basin. Conversely, surface Mn concentration changes in the Canada Basin are an indicator of the volume of sediments released by sea ice melt. Sea ice loss is calculated from regional monthly sea ice area changes in the Beaufort Sea measured by the Defense Meteorological Satellite Program series of passive microwave remote sensing instruments (Fetterer et al., 2017). The regional Mn model presented in this study is used to calculate Mn added by sea ice melt and the total Mn content of the Canada Basin.

Sea ice contributes around 34% of net Mn transported from Parry Channel into Baffin Bay. The reduction in the contribution of these components does not indicate loss in the CAA; it reflects the additional contributions from other sources (mainly sediment resuspension) in the CAA. The sea ice contribution in the water column is significant downstream, however, it is important to note that the sea ice transport in the CAA in the ocean-ice model is stronger than observed due to the lack of a land-fast ice parameterization (Grivault et al., 2018). As a result, we may overestimate the sea ice transport and thus melt in Parry Channel, particularly for the outflow from Parry Channel into Baffin Bay. There are also further factors contributing Mn within the CAA which confound this finding. The acceleration of the hydrological cycle and permafrost thaw may increase the contributions of riverine Mn to the CAA; our experiments do not take these changes into account. On the other hand, sea ice melt is associated with an increase in stratification which may reduce the depth up to which resuspended sediment can mix, reducing the Mn supplied into the upper water column (and productive areas) by sediment resuspension in the CAA. However, reduced sea ice cover is also associated with increased wind-driven mixing.

Our findings for Mn in the Arctic have implications for nutrients which share similar sources. In the Arctic Ocean, iron (Fe) behaves similarly to Mn, although Fe is less soluble than Mn and oxidizes more rapidly (Landing and Bruland (1987); Colombo et al. (2020); for a comprehensive discussion, read Jensen et al. (2020)). Fe is an essential micronutrient and in some regions of the ocean, such as the Southern Ocean, parts of the North Atlantic, and the Pacific Northwest, it limits primary productivity (Martin & Gordon, 1988; Hawkings et al., 2014; Tagliabue et al., 2017). Generally, iron is not growth limiting in the Arctic (S. Wang et al., 2014), but there is evidence that Fe is limited in some specific regions: on the outer shelf and shelf break in the Bering Sea (Aguilar-Islas et al., 2008), as well as in the Barents Sea and Nansen Basin (Rijkenberg et al., 2018). Past studies have indicated that sea ice contributes to the flux of Fe into the ocean (Measures, 1999; Lannuzel et al., 2007; Aguilar-Islas et al., 2008; Kanna et al., 2020). Based on the expected changes to the Mn cycle and supply with sea ice melt over the next decades, the supply of Fe to the Canada Basin may be reduced as well. Meanwhile, the increase in simulated Mn content in the Canada Basin from 2002-2019 due to sea ice melt may also have supplied micronutrients such as Fe and have driven some of the observed increased Arctic Ocean primary production (Lewis et al., 2020). Changes to Fe availabil-

784 ity impact the community composition and the timing of the spring phytoplankton bloom

785 (Aguilar-Islas et al., 2008), which in turn has consequences for biological productivity,

786 Arctic ecosystems, and the carbon cycle.

4.3 Limitations of Results

4.3.1 Mn model evaluation

789 The upper 100 m of the water column are most important to the key findings of

790 this study. In this zone, the Mn representation is impacted by local sources, photo-enhanced

791 reduction, and the physical model's salinity representation and associated mixing. Be-

792 low, we discuss differences between the model and observations and identify the impacts

793 on our findings.

794 In the CAA, the model underestimates Mn in the subsurface (upper 50 m) result-

795 ing in a strong vertical gradient of Mn, particularly in the central sills region. The phys-

796 ical model represents salinity well within the CAA, however the upper 20 m are slightly

797 too fresh, possibly because of an overestimate in the freshwater transport due to too-mobile

798 sea ice without a land-fast sea ice parameterization (Grivault et al., 2018). Despite this,

799 the Mn-salinity relationship matches observations closely in the reference experiment (Fig. S9a).

800 Increased photo-enhanced reduction could increase subsurface Mn, however, trials with

801 a non-linear coupling between light penetration and sea ice concentration did not sig-

802 nificantly affect the subsurface Mn concentrations. Further, while Mn oxides (oMn) are

803 only modelled for their impact on dMn, oMn concentrations are fairly well-represented

804 within the upper water column in the CAA (Fig. S8). Remineralization of Mn taken up

805 by phytoplankton may also counteract some of the subsurface underestimation. How-

806 ever, we estimated that uptake and remineralization altered dissolved Mn profiles by only

807 up to 0.3 nM (Fig. S15 and Text S3). Hence, we suggest that the subsurface Mn under-

808 estimation is most likely caused by improper distribution of materials in the upper wa-

809 ter column from weaker mixing. Replicating the effect of stronger mixing by redistribut-

810 ing the Mn, the average Mn concentrations are underestimated by 1 nM in the upper

811 50 m, while in the subsurface alone they are underestimated by 3 nM. A similar argu-

812 ment can be made for the near-bottom overestimation of Mn at CAA9; a region known

813 to have strong tidal mixing. If we redistribute the Mn throughout the water column, the

modelled concentration is overestimated by 2 nM, compared to 5 nM for the lower water column alone.

In the Canada Basin, the physical model captures the depth of isohalines reasonably well, however the amount of freshwater in the upper water column is underestimated (Hu et al., 2019). This underestimation may be due to to a lower freshwater state in the initial conditions derived from the GLORYS2v3 product, but can more likely be attributed to overestimated sea ice concentration and thickness (and so, underestimated melt in the model). Despite this, the model represents the overall circulation and characteristics of the Canada Basin. For Mn, this shortcoming complicates the evaluation of the Mn-salinity relationship in the Canada Basin (Fig. S9) and instead, we focused our evaluation on Mn with depth (Fig. 5). The underestimation of sea ice melt does not change the actual component contributions estimated by the Mn model: the net effect of the sea ice component is a combination of ice melt and sediment content, so an increase in melt would be counterbalanced by a decrease in sediment richness. The exact spatial variability and content of sediment in sea ice of the forcing field is a rough first order estimate, nevertheless it is able to provide us with an estimate of the magnitude of the sediment in sea ice component.

4.3.2 Parameterizations

The findings in this study are limited by the parameterizations for scavenging, sediment in sea ice, sediment resuspension, and river runoff. Overall, the model is best constrained for summer months, the southern CAA, and the Canada Basin due to the availability of observations. Scavenging rates are important throughout the water column and are most likely to affect our results in coastal regions. We assumed steady state to estimate the adsorption and desorption rates from observations; this assumption is least likely to hold in coastal regions and near the surface where scavenging rates are both important and variable. For the sediment released by sea ice, we did not account for variations in transport of sediment (and its origin) across the Arctic Ocean over the course of the time series. Sea ice drift patterns vary interannually, and so could the source regions for sediment transported to the Canada Basin by sea ice. The sediment content would more accurately be represented as a time dependent variable. The total Mn content in the Canada Basin would increase (decrease) with a higher (lower) sediment content in sea ice, while sediment in sea ice would be more (less) important overall. How-

ever, observed sediment sea ice loads range several orders of magnitude by location sampled and properties of the ice, and these fluctuations make it challenging to quantify annual changes in overall sediment content and path travelled. Similarly, sediment resuspension varies interannually and seasonally and may be better represented as a time dependent variable.

We do not take into account the contributions from breaking of internal waves, storm generated currents, and surface waves on sediment resuspension and coastal erosion. As a result, we likely underestimate sediment resuspension contributions in some areas, particularly during the summer ice-free period. Our treatment of rivers was simplistic and did not account for the complexity of transformations that occur in the estuarine zone. Our results indicate a lower and upper bound of the river contributions, however we are unable to indicate what the actual contribution is. We also did not account for the projected seasonal ranges in riverine Mn concentrations with discharge (Colombo et al., 2019); the river discharge varies seasonally, but we hold the characteristic Mn concentrations of the rivers constant. This approximation could underestimate the riverine contributions during the spring freshet in coastal areas and is most likely to impact the northern CAA and Greenland coast, where glacial rivers are most important.

While the numbers presented here should be taken as an estimate of magnitude rather than as exact values, the key results are robust to the uncertainties described above. The only way we were able to close the Mn budget (particularly in the Canada Basin) was by incorporating the sediment in sea ice component. Similarly, the only way to represent the higher concentrations of Mn found in the lower water column at some stations in the CAA was through the sediment resuspension term. While the Mn model presented here is limited in its representation of these processes, it provides a platform to ask questions about the drivers of Mn variability and to perform larger scale estimates of the processes that contribute Mn to the Arctic Ocean. Improvements to the estimates of sediment content in sea ice from, for example, satellite products would strengthen future predictions, while the model accuracy would be improved by more comprehensive estimates of the scavenging and sediment resuspension rates. Observations of Mn along a transect from an estuary into the ocean would help constrain the riverine contributions.

5 Conclusions

New trace metal datasets collected in the Arctic Ocean as part of the Canadian GEO-TRACES program have provided an essential base for studying biogeochemical cycling in this unique region. Using in situ observations from Colombo et al. (2020), we developed the first model of Mn in the Canadian Arctic Archipelago and the Canada Basin. With three experiments from 2002-2019, we looked at (1) the drivers of Mn distributions in the CAA and the Canada Basin and (2) implications of future sea ice transport changes on the biogeochemical cycles of nutrients in the Arctic Ocean.

(1) While sediment transport by sea ice is identified as important in the Arctic Ocean (Measures, 1999; Eicken et al., 2005), this mechanism is commonly considered less significant for Mn than riverine input. However, without the contribution from sediment in sea ice to Mn, we were unable to accurately represent the Mn concentrations in the Canada Basin with our model. Sediments transported in sea ice by the transpolar drift account for up to 93% of the total annual Mn added in the Canada Basin and up to 37% in the CAA, driving Mn surface maxima. These results support the hypothesis that "ice-rafted sediment may be an important transport mechanism for supplying reactive trace elements," proposed by Measures (1999). Rivers are certainly locally important, but contribute only 2.2 (8.5)% annually in the Canada Basin. Within the CAA, our estimates for river contributions ranged from 5.0% up to 34% in the upper bound river experiment. This broad range is the result of the limited information available regarding estuarine cycling in the Arctic. A clear divide is present in the CAA: west of Barrow Sill, the mean concentrations are lower and the behaviour of Mn is more similar to the Canada Basin, while in the eastern CAA, sediments resuspended by high tidal speeds, as well as many glacial rivers drive higher Mn concentrations.

(2) Sea ice transport via the transpolar drift is interrupted by Arctic warming (Krumpen et al., 2019) and the decline in this long range transport could reduce the Canada Basin and the CAA nutrient supply. These changes not only impact the Arctic, but also sub-arctic seas, with up to 34% of the Mn transported from Parry Channel into Baffin Bay added by sea ice melt. Mn behaves similarly to Fe in the Arctic Ocean and both of these micronutrients support phytoplankton growth. The importance of sea ice for nutrient supply to the photic zone in the Canada Basin, as well as downstream, is concerning given the recent changes in the Arctic Ocean sea ice regime (reduced summer min-

imum ice extent, ice thinning, reduction in multi-year ice extent, and altered drift paths). There are many competing factors that will contribute to changes in the biogeochemical cycles; combined model-observation studies are highly valuable to understand the individual contribution of these factors.

Acronyms

CAA Canadian Arctic Archipelago

NEMO Nucleus for European Modelling of the Ocean

ANHA12 Arctic and Northern Hemispheric Atlantic 1/12 degree

LIM2 Louvain-la-Neuve version 2

TOP Tracers in the Ocean Paradigm

TVD Total Variance Dissipation scheme

CESM Community Earth System Model

CAM-Chem Community Atmosphere Model with Chemistry

References

Aguilar-Islas, A. M., Rember, R. D., Mordy, C. W., & Wu, J.   (2008).   Sea ice-
derived dissolved iron and its potential influence on the spring algal bloom in

the Bering Sea. *Geophys. Res. Lett.*, *35*(24). doi: 10.1029/2008GL035736

Bacon, S., Marshall, A., Holliday, N. P., Aksenov, Y., & Dye, S. R. (2014). Seasonal variability of the East Greenland Coastal Current. *J. Geophys. Res.-Ocean.*, *119*(6), 3967–3987. doi: 10.1002/2013JC009279

Balzer, W. (1982). On the distribution of iron and manganese at the sediment/water interface: Thermodynamic versus kinetic control. *Geochem. Cosmochim. Acta*, *46*(7), 1153–1161. doi: 10.1016/0016-7037(82)90001-1

Bamber, J., Van Den Broeke, M., Ettema, J., Lenaerts, J., & Rignot, E. (2012). Recent large increases in freshwater fluxes from Greenland into the North Atlantic. *Geophys. Res. Lett.*, *39*(19). doi: 10.1029/2012GL052552

Bhatia, M. P., Waterman, S., Burgess, D. O., Williams, P. L., Bundy, R. M., Mellett, T., . . . Bertrand, E. M. (2021). Glaciers and Nutrients in the Canadian Arctic Archipelago Marine System. *Global Biogeochem. Cycles*, *35*, e2021GB006976. doi: 10.1029/2021GB006976

Bouillon, S., Morales Maqueda, M. A., Legat, V., & Fichefet, T. (2009). An elastic-viscous-plastic sea ice model formulated on Arakawa B and C grids. *Ocean Model.*, *27*(3-4), 174–184. doi: 10.1016/j.ocemod.2009.01.004

Brand, L. E., Sunda, W. G., & Guillard, R. R. L. (1983). Limitation of marine phytoplankton reproductive rates by zinc, manganese, and iron. *Limnol. Oceanogr.*, *28*(6), 1182–1198. doi: 10.4319/lo.1983.28.6.1182

Brown, K. A., Williams, W. J., Carmack, E. C., Fiske, G., François, R., McLennan, D., & Peucker-Ehrenbrink, B. (2020). Geochemistry of small Canadian Arctic rivers with diverse geological and hydrological settings. *J. Geophys. Res.-Biogeosciences*, *125*(1). doi: 10.1029/2019JG005414

Bruland, K. W., Donat, J. R., & Hutchins, D. A. (1991). Interactive influences of bioactive trace metals on biological production in oceanic waters. *Limnol. Oceanogr.*, *36*(8), 1555–1577. doi: 10.4319/lo.1991.36.8.1555

Bruland, K. W., Orians, K. J., & Cowen, J. P. (1994). Reactive trace metals in the stratified central North Pacific. *Geochem. Cosmochim. Acta*, *58*(15), 3171–3182. doi: 10.1016/0016-7037(94)90044-2

Campbell, J. A., & Yeats, P. A. (1982). The distribution of manganese, iron, nickel, copper and cadmium in the waters of Baffin Bay and the Canadian Arctic Archipelago. *Oceanol. Acta*, *5*(2), 161–168.

Carrère, L., & Lyard, F. (2003). Modeling the barotropic response of the global ocean to atmospheric wind and pressure forcing-comparisons with observations. *Geophys. Res. Lett.*, *30*(6). doi: 10.1029/2002GL016473

Charette, M. A., Kipp, L. E., Jensen, L. T., Dabrowski, J. S., Whitmore, L. M., Fitzsimmons, J. N., ... others (2020). The Transpolar Drift as a source of riverine and shelf-derived trace elements to the central Arctic Ocean. *J. Geophys. Res.-Ocean.*, *125*(5). doi: 10.1029/2019jc015920

Charette, M. A., Lam, P. J., Lohan, M. C., Kwon, E. Y., Hatje, V., Jeandel, C., ... Garcia-Orellana, J. (2016). Coastal ocean and shelf-sea biogeochemical cycling of trace elements and isotopes: lessons learned from GEOTRACES. *Philos. Trans. Roy. Soc. A*, *374*(2081), 20160076. doi: 10.1098/rsta.2016.0076

Chelton, D. B., de Szoeke, R. A., Schlax, M. G., El Naggar, K., & Siwertz, N. (1998). Geographical variability of the first baroclinic Rossby radius of deformation. *J. Phys. Oceangr.*, *28*(3), 433–460. doi: 10.1175/1520-0485(1998)028%3C0433:GVOTFB%3E2.0.CO;2

Cid, A. P., Nakatsuka, S., & Sohrin, Y. (2012). Stoichiometry among bioactive trace metals in the Chukchi and Beaufort Seas. *J. Oceanogr.*, *68*(6), 985–1001. doi: 10.1007/s10872-012-0150-8

Colombo, M., Brown, K. A., De Vera, J., Bergquist, B. A., & Orians, K. J. (2019). Trace metal geochemistry of remote rivers in the Canadian Arctic Archipelago. *Chem. Geol.*, *525*, 479–491. doi: 10.1016/j.chemgeo.2019.08.006

Colombo, M., Jackson, S. L., Cullen, J. T., & Orians, K. J. (2020). Dissolved iron and manganese in the Canadian Arctic Ocean: on the biogeochemical processes controlling their distributions. *Geochem. Cosmochim. Acta*, *277*, 150–174. doi: 10.1016/j.gca.2020.03.012

Colombo, M., Rogalla, B., Li, J., Allen, S. E., Orians, K. J., & Maldonado, M. T. (2021). Canadian Arctic Archipelago Shelf-Ocean Interactions: A Major Iron Source to Pacific Derived Waters Transiting to the Atlantic. *Global Biogeochem. Cycles*, *35*(10), e2021GB007058. doi: 10.1029/2021GB007058

Dai, A., Qian, T., Trenberth, K. E., & Milliman, J. D. (2009). Changes in continental freshwater discharge from 1948 to 2004. *J. Climate*, *22*(10), 2773–2792. doi: 10.1175/2008JCLI2592.1

Damm, E., Bauch, D., Krumpen, T., Rabe, B., Korhonen, M., Vinogradova, E.,

& Uhlig, C. (2018). The Transpolar Drift conveys methane from the Siberian Shelf to the central Arctic Ocean. *Sci. Rep.*, *8*(1), 1–10. doi: 10.1038/s41598-018-22801-z

Darby, D. A., Myers, W. B., Jakobsson, M., & Rigor, I. (2011). Modern dirty sea ice characteristics and sources: The role of anchor ice. *J. Geophys. Res.-Ocean.*, *116*(9). doi: 10.1029/2010JC006675

D'Asaro, E. A., & Morison, J. H. (1992). Internal waves and mixing in the Arctic Ocean. *Deep Sea Res. Pt. I*, *39*(2), S459–S484. doi: 10.1016/S0198-0149(06) 80016-6

Dethleff, D., & Kuhlmann, G. (2009). Entrainment of fine-grained surface deposits into new ice in the southwestern Kara Sea, Siberian Arctic. *Cont. Shelf Res.*, *29*(4), 691–701. doi: 10.1016/j.csr.2008.11.009

Dethleff, D., & Kuhlmann, G. (2010). Fram Strait sea-ice sediment provinces based on silt and clay compositions identify Siberian Kara and Laptev seas as main source regions. *Polar Sci.*, *29*(3). doi: 10.3402/polar.v29i3.6070

Dethleff, D., Rachold, V., Tintelnot, M., & Antonow, M. (2000). Sea-ice transport of riverine particles from the Laptev Sea to Fram Strait based on clay mineral studies. *Intl. J. Earth Sci.*, *89*(3), 496–502. doi: 10.1007/s005310000109

Drinkwater, K. F., & Harding, G. C. (2001). Effects of the Hudson Strait outflow on the biology of the Labrador Shelf. *Can. J. Fish. Aquat. Sci.*, *58*(1), 171–184. doi: 10.1139/f00-210

Eicken, H., Gradinger, R., Gaylord, A., Mahoney, A., Rigor, I., & Melling, H. (2005). Sediment transport by sea ice in the Chukchi and Beaufort Seas: Increasing importance due to changing ice conditions? *Deep Sea Res. Pt. II*, *52*, 3281–3302. doi: 10.1016/j.dsr2.2005.10.006

Eicken, H., Kolatschek, J., Freitag, J., Lindemann, F., Kassens, H., & Dmitrenko, I. (2000). A key source area and constraints on entrainment for basin-scale sediment transport by Arctic sea ice. *Geophys. Res. Lett.*, *27*(13), 1919–1922. doi: 10.1029/1999GL011132

Eicken, H., Reimnitz, E., Alexandrov, V., Martin, T., Kassens, H., & Viehoff, T. (1997). Sea-ice processes in the Laptev Sea and their importance for sediment export. *Cont. Shelf Res.*, *17*(2), 205–233. doi: 10.1016/ S0278-4343(96)00024-6

Epstein, J.-L. (2018). *The impact of internal tide mixing parameterizations in an eddy-permitting model of the Arctic Ocean* (Master's thesis, University of British Columbia). doi: 10.14288/1.0365809

Evans, L. K., & Nishioka, J. (2018). Quantitative analysis of Fe, Mn and Cd from sea ice and seawater in the Chukchi Sea, Arctic Ocean. *Polar Sci.*, *17*, 50–58. doi: 10.1016/j.polar.2018.07.002

Fetterer, F., Knowles, K., Meier, W. N., Savoie, M., & Windnagel, A. K. (2017). Updated daily: Sea ice index, version 3. Boulder, Colorado USA. *NSIDC: National Snow and Ice Data Center*. doi: 10.7265/N5K072F8

Fichefet, T., & Maqueda, M. A. M. (1997). Sensitivity of a global sea ice model to the treatment of ice thermodynamics and dynamics. *J. Geophys. Res.-Ocean.*, *102*(C6), 12609–12646. doi: 10.1029/97JC00480

Fichot, C. G., Kaiser, K., Hooker, S. B., Amon, R. M., Babin, M., Bélanger, S., . . . Benner, R. (2013). Pan-Arctic distributions of continental runoff in the Arctic Ocean. *Sci. Rep.*, *3*(1), 1–6. doi: 10.1038/srep01053

Fishwick, M. P., Ussher, S. J., Sedwick, P. N., Lohan, M. C., Worsfold, P. J., Buck, K. N., & Church, T. M. (2018). Impact of surface ocean conditions and aerosol provenance on the dissolution of aerosol manganese, cobalt, nickel and lead in seawater. *Mar. Chem.*, *198*, 28–43. doi: 10.1016/J.MARCHEM.2017.11.003

Gent, P. R., Willebrand, J., McDougall, T. J., & McWilliams, J. C. (1995). Parameterizing eddy-induced tracer transport in ocean circulation models. *J. Phys. Oceangr.*, *25*(4), 463–474. doi: 10.1175/1520-0485(1995)025%3C0463:PEITTI%3E2.0.CO;2

Granskog, M. A., Kaartokallio, H., & Shirasawa, K. (2003). Nutrient status of Baltic Sea ice: Evidence for control by snow-ice formation, ice permeability, and ice algae. *J. Geophys. Res.-Ocean.*, *108*(C8). doi: 10.1029/2002jc001386

Greene, C. H., & Pershing, A. J. (2007). Climate drives sea change. *Science*, *315*(5815), 1084–1085. doi: 10.1126/science.1136495

Grivault, N., Hu, X., & Myers, P. G. (2018). Impact of the surface stress on the volume and freshwater transport through the Canadian Arctic Archipelago from a high-resolution numerical simulation. *J. Geophys. Res.-Ocean.*, *123*(12), 9038–9060. doi: 10.1029/2018JC013984

Guay, C. K. H., McLaughlin, F. A., & Yamamoto-Kawai, M. (2009). Differentiating

fluvial components of upper Canada Basin waters on the basis of measurements of dissolved barium combined with other physical and chemical tracers. *J. Geophys. Res.-Ocean.*, *114*(C1). doi: 10.1029/2008JC005099

Hawkings, J. R., Wadham, J. L., Tranter, M., Raiswell, R., Benning, L. G., Statham, P. J., ... Telling, J. (2014). Ice sheets as a significant source of highly reactive nanoparticulate iron to the oceans. *Nat. Commun.*, *5*(1), 1–8. doi: 10.1038/ncomms4929

Hayashida, H., Christian, J. R., Holdsworth, A. M., Hu, X., Monahan, A. H., Mortenson, E., ... Steiner, N. S. (2019). CSIB v1 (Canadian Sea-ice Biogeochemistry): a sea-ice biogeochemical model for the NEMO community ocean modelling framework. *Geosci. Model Dev.*, *12*(5), 1965-1990. doi: 10.5194/gmd-12-1965-2019

Hölemann, J., Wegener, A., & Schirmacher, M. (1999). Dissolved and particulate major and trace elements in newly formed ice from the Laptev Sea (Transdrift III, October 1995). In *Land-ocean systems in the Siberian Arctic* (pp. 101–111). Springer Berlin Heidelberg. doi: 10.1007/978-3-642-60134-7_11

Holland, M. M., Bailey, D. A., Briegleb, B. P., Light, B., & Hunke, E. (2012). Improved sea ice shortwave radiation physics in CCSM4: The impact of melt ponds and aerosols on Arctic sea ice. *J. Climate*, *25*(5), 1413–1430. doi: 10.1175/JCLI-D-11-00078.1

Hu, X., Myers, P. G., & Lu, Y. (2019). Pacific water pathway in the Arctic Ocean and Beaufort Gyre in two simulations with different horizontal resolutions. *J. Geophys. Res.-Ocean.*, *124*(8), 6414–6432. doi: 10.1029/2019JC015111

Hu, X., Sun, J., Chan, T. O., & Myers, P. G. (2018). Thermodynamic and dynamic ice thickness contributions in the Canadian Arctic Archipelago in NEMO-LIM2 numerical simulations. *Cryosphere*, *12*, 1233–1247. doi: 10.5194/tc-12-1233-2018

Hughes, K. G., Klymak, J. M., Hu, X., & Myers, P. G. (2017). Water mass modification and mixing rates in a 1/12 simulation of the Canadian Arctic Archipelago. *J. Geophys. Res.-Ocean.*, *122*, 803–820. doi: 10.1002/2016JC012235

Hughes, K. G., Klymak, J. M., Williams, W. J., & Melling, H. (2018). Tidally modulated internal hydraulic flow and energetics in the central Canadian

Arctic Archipelago. *J. Geophys. Res.-Ocean., 123*(8), 5210–5229. doi: 10.1029/2018JC013770

Hunter, J. D. (2007). Matplotlib: A 2d graphics environment. *Comput. Sci. Eng., 9*(3), 90–95.

Jakobsson, M. (2002). Hypsometry and volume of the Arctic Ocean and its constituent seas. *Geochem. Geophys. Geosystems, 3*(5), 1–18. doi: 10.1029/2001GC000302

Jensen, L. T., Morton, P., Twining, B. S., Heller, M. I., Hatta, M., Measures, C. I., ... Fitzsimmons, J. N. (2020). A comparison of marine Fe and Mn cycling: U.S. GEOTRACES GN01 Western Arctic case study. *Geochem. Cosmochim. Acta*. doi: 10.1016/j.gca.2020.08.006

Johnson, K. S., Coale, K. H., Berelson, W. M., & Michael Gordon, R. (1996). On the formation of the manganese maximum in the oxygen minimum. *Geochem. Cosmochim. Acta, 60*(8), 1291–1299. doi: 10.1016/0016-7037(96)00005-1

Kanna, N., Lannuzel, D., van der Merwe, P., & Nishioka, J. (2020). Size fractionation and bioavailability of iron released from melting sea ice in a subpolar marginal sea. *Mar. Chem., 221*, 103774. doi: 10.1016/j.marchem.2020.103774

Kay, J. E., Deser, C., Phillips, A., Mai, A., Hannay, C., Strand, G., ... Vertenstein, M. (2015). The community earth system model (CESM) large ensemble project : A community resource for studying climate change in the presence of internal climate variability. *B. Am. Meteorol. Soc., 96*(8), 1333–1349. doi: 10.1175/BAMS-D-13-00255.1

Kelly, S. J., Proshutinsky, A., Popova, E. K., Aksenov, Y. K., & Yool, A. (2019). On the origin of water masses in the Beaufort Gyre. *J. Geophys. Res.-Ocean., 124*(7), 4696–4709. doi: 10.1029/2019JC015022

Kempema, E. W., Reimnitz, E., & Barnes, P. (1989). Sea ice sediment entrainment and rafting in the Arctic. *J. Sediment. Petrol., 59*(2), 308–317. doi: 10.1306/212F8F80-2B24-11D7-8648000102C1865D

Kipp, L. E., Charette, M. A., Moore, W. S., Henderson, P. B., & Rigor, I. G. (2018). Increased fluxes of shelf-derived materials to the central Arctic Ocean. *Sci. Advances, 4*(1). doi: 10.1126/sciadv.aao1302

Klinkhammer, G. P., & Bender, M. L. (1980). The distribution of manganese in the Pacific Ocean. *Earth Planet Sc. Lett., 46*(3), 361–384. doi: 10.1016/0012

-821X(80)90051-5

Kluyver, T., Ragan-Kelley, B., Pérez, F., Granger, B., Bussonnier, M., Frederic, J., ... others (2016). *Jupyter notebooks – a publishing format for reproducible computational workflows* (F. Loizides & B. Schmidt, Eds.). IOS Press.

Kodaira, T., Waseda, T., Nose, T., & Inoue, J. (2020). Record high Pacific Arctic seawater temperatures and delayed sea ice advance in response to episodic atmospheric blocking. *Sci. Rep.*, *10*(1), 1–12.

Kondo, Y., Obata, H., Hioki, N., Ooki, A., Nishino, S., Kikuchi, T., & Kuma, K. (2016). Transport of trace metals (Mn, Fe, Ni, Zn and Cd) in the western Arctic Ocean (Chukchi Sea and Canada Basin) in late summer 2012. *Deep Sea Res. Pt. I*, *116*, 236–252. doi: 10.1016/J.DSR.2016.08.010

Krachler, M., Zheng, J., Fisher, D., & Shotyk, W. (2005). Analytical procedures for improved trace element detection limits in polar ice from Arctic Canada using ICP-SMS. *Anal. Chim. Acta*, *530*(2), 291–298. doi: 10.1016/j.aca.2004.09.024

Krishfield, R. A., Proshutinsky, A., Tateyama, K., Williams, W. J., Carmack, E. C., McLaughlin, F. A., & Timmermans, M. L. (2014). Deterioration of perennial sea ice in the Beaufort Gyre from 2003 to 2012 and its impact on the oceanic freshwater cycle. *J. Geophys. Res.-Ocean.*, *119*(2), 1271–1305. doi: 10.1002/2013JC008999

Krumpen, T., Belter, H. J., Boetius, A., Damm, E., Haas, C., Hendricks, S., ... Stein, R. (2019). Arctic warming interrupts the Transpolar Drift and affects long-range transport of sea ice and ice-rafted matter. *Sci. Rep.*, *9*(1), 1–9. doi: 10.1038/s41598-019-41456-y

Kuss, J., & Kremling, K. (1999). Spatial variability of particle associated trace elements in near-surface waters of the North Atlantic (30 N/60 W to 60 N/2 W), derived by large volume sampling. *Mar. Chem.*, *68*(1-2), 71–86. doi: 10.1016/S0304-4203(99)00066-3

Kwok, R., Spreen, G., & Pang, S. (2013). Arctic sea ice circulation and drift speed: Decadal trends and ocean currents. *J. Geophys. Res.-Ocean.*, *118*(5), 2408–2425. doi: 10.1002/jgrc.20191

Landing, W. M., & Bruland, K. W. (1987). The contrasting biogeochemistry of iron and manganese in the Pacific Ocean. *Geochem. Cosmochim. Acta*, *51*(1), 29–43. doi: 10.1016/0016-7037(87)90004-4

1168   Laney, S. R., Krishfield, R. A., & Toole, J. M.   (2017, 9).   The euphotic zone under
1169   Arctic Ocean sea ice: Vertical extents and seasonal trends.   *Limnol. Oceanogr.*,
1170   *62*, 1910-1934. doi: 10.1002/LNO.10543

1171   Lange, M., & Van Sebille, E.   (2017).   Parcels v0.9: Prototyping a Lagrangian ocean
1172   analysis framework for the petascale age.   *Geosci. Model Dev.*, *10*(11), 4175–
1173   4186. doi: 10.5194/gmd-10-4175-2017

1174   Lannuzel, D., Schoemann, V., de Jong, J., & Tison, J.-L.   (2007).   Distribution and
1175   biogeochemical behaviour of iron in the East Antarctic sea ice.   *Mar. Chem.*,
1176   *106*(1-2), 18–32. doi: 10.1016/J.MARCHEM.2006.06.010

1177   Lavelle, J. W., Cowen, J. P., & Massoth, G. J.   (1992).   A model for the deposition
1178   of hydrothermal manganese near ridge crests.   *J. Geophys. Res.*, *97*(C5), 7413.
1179   doi: 10.1029/92JC00406

1180   Lévy, M., Estublier, A., & Madec, G.   (2001).   Choice of an advection scheme for bio-
1181   geochemical models.   *Geophys. Res. Lett.*, *28*(19), 3725–3728.   doi: 10.1029/
1182   2001GL012947

1183   Lewis, K. M., van Dijken, G. L., & Arrigo, K. R.   (2020).   Changes in phytoplankton
1184   concentration now drive increased Arctic Ocean primary production.   *Science*,
1185   *369*(6500), 198–202. doi: 10.1126/science.aay8380

1186   Li, J.   (2017).   *Particulate trace metals and iron availability to phytoplankton in a*
1187   *changing Arctic Ocean* (Master's thesis, University of British Columbia).   doi:
1188   10.14288/1.0348666

1189   Liang, X., & Losch, M.   (2018).   On the effects of increased vertical mixing on the
1190   Arctic Ocean and sea ice.   *J. Geophys. Res.-Ocean.*, *123*(12).   doi: 10.1029/
1191   2018JC014303

1192   Macdonald, R. W., & Gobeil, C.   (2012).   Manganese sources and sinks in the Arc-
1193   tic Ocean with reference to periodic enrichments in basin sediments.   *Aquat.*
1194   *Geochem.*, *18*(6), 565–591. doi: 10.1007/s10498-011-9149-9

1195   Madec, G.   (2008).   NEMO ocean engine.   *Note du Pôle de modélisation, Insti-*
1196   *tut Pierre-Simon Laplace*, *27*(1288-1619).   Retrieved from https://www.nemo
1197   -ocean.eu/wp-content/uploads/NEMO_book.pdf

1198   Martin, J. H., & Gordon, R. M.   (1988).   Northeast Pacific iron distributions in rela-
1199   tion to phytoplankton productivity. *Deep Sea Res. Pt. I*, *35*(2), 177–196.   doi:
1200   10.1016/0198-0149(88)90035-0

Masina, S., Storto, A., Ferry, N., Valdivieso, M., Haines, K., Balmaseda, M., ... Parent, L. (2017). An ensemble of eddy-permitting global ocean reanalyses from the MyOcean project. *Clim. Dynam.*, *49*(3), 813–841. doi: 10.1007/s00382-015-2728-5

Measures, C. I. (1999). The role of entrained sediments in sea ice in the distribution of aluminium and iron in the surface waters of the Arctic Ocean. *Mar. Chem.*, *68*, 59–70. doi: 10.1016/S0304-4203(99)00065-1

Michel, C., Ingram, R. G., & Harris, L. R. (2006, 10). Variability in oceanographic and ecological processes in the canadian arctic archipelago. *Prog. Oceanogr.*, *71*, 379-401. doi: 10.1016/J.POCEAN.2006.09.006

Middag, R., de Baar, H. J. W., Laan, P., Cai, P. H., & van Ooijen, J. C. (2011a). Dissolved manganese in the Atlantic sector of the Southern Ocean. *Deep Sea Res. Pt. II*, *58*(25-26), 2661–2677. doi: 10.1016/J.DSR2.2010.10.043

Middag, R., de Baar, H. J. W., Laan, P., & Klunder, M. B. (2011b). Fluvial and hydrothermal input of manganese into the Arctic Ocean. *Geochem. Cosmochim. Acta*, *75*(9), 2393–2408. doi: 10.1016/J.GCA.2011.02.011

Newton, R., Pfirman, S., Tremblay, B., & DeRepentigny, P. (2017). Increasing transnational sea-ice exchange in a changing Arctic Ocean. *Earths Future*, *5*(6), 633–647. doi: 10.1002/2016EF000500

Nürnberg, D., Wollenburg, I., Dethleff, D., Eicken, H., Kassens, H., Letzig, T., & Reimnitz, E. (1994). Sediments in Arctic sea ice: Implications for entrainment, transport and release. *Mar. Geol.*, *119*, 185–214. doi: 10.1016/0025-3227(94)90181-3

O'Brien, M. C., Macdonald, R. W., Melling, H., & Iseki, K. (2006). Particle fluxes and geochemistry on the Canadian Beaufort Shelf: Implications for sediment transport and deposition. *Cont. Shelf Res.*, *26*(1), 41–81. doi: 10.1016/J.CSR.2005.09.007

Oliphant, T. E. (2006). *A guide to numpy* (Vol. 1). Trelgol Publishing USA.

Pedregosa, F., Varoquaux, G., Gramfort, A., Michel, V., Thirion, B., Grisel, O., ... Duchesnay, E. (2011). Scikit-learn: Machine learning in Python. *J. Mach.*, *12*, 2825–2830.

Peeken, I., Primpke, S., Beyer, B., Gütermann, J., Katlein, C., Krumpen, T., ... Gerdts, G. (2018). Arctic sea ice is an important temporal sink and

means of transport for microplastic. *Nat. Commun.*, *9*(1), 1–12. doi: 10.1038/s41467-018-03825-5

Pfirman, S. L., Eicken, H., Bauch, D., & Weeks, W. (1995). The potential transport of pollutants by Arctic sea ice. *Sci. Total Environ.*, *159*(2-3), 129–146. doi: 10.1016/0048-9697(95)04174-Y

Proshutinsky, A., Krishfield, R., Toole, J. M., Timmermans, M. L., Williams, W., Zimmermann, S., ... Zhao, J. (2019). Analysis of the Beaufort Gyre freshwater content in 2003–2018. *J. Geophys. Res.-Ocean.*, *124*(12), 9658–9689. doi: 10.1029/2019JC015281

Reimnitz, E., Mccormick, M., Mcdougall, K., & Brouwers, E. (1993). Sediment export by ice rafting from a coastal polynya. *Arct. Antarct. Alp. Res.*, *25*(2), 83–98. doi: 10.1080/00040851.1993.12002988

Rijkenberg, M. J. A., Slagter, H. A., van der Loeff, M., van Ooijen, J., & Gerringa, L. J. A. (2018). Dissolved Fe in the deep and upper Arctic Ocean with a focus on Fe limitation in the Nansen Basin. *Front. Mar. Sci.*, *5*, 88. doi: 10.3389/fmars.2018.00088

Roy-Barman, M. (2009). Modelling the effect of boundary scavenging on Thorium and Protactinium profiles in the ocean. *Biogeosciences*, *6*, 3091-3107. doi: 10.5194/bg-6-3091-2009

Sim, N. (2018). *Biogeochemical cycling of dissolved and particulate manganese in the northeast Pacific and Canadian western Arctic* (Doctoral dissertation, University of British Columbia). doi: 10.14288/1.0374222

Smith, G. C., Roy, F., Mann, P., Dupont, F., Brasnett, B., Lemieux, J.-F., ... Bélair, S. (2014). A new atmospheric dataset for forcing ice-ocean models: Evaluation of reforecasts using the Canadian global deterministic prediction system. *Q. J. R. Meteorol. Soc.*, *140*(680), 881–894. doi: 10.1002/qj.2194

Spreen, G., Kwok, R., & Menemenlis, D. (2011). Trends in Arctic sea ice drift and role of wind forcing: 1992-2009. *Geophys. Res. Lett.*, *38*(19). doi: 10.1029/2011GL048970

Stierle, A. P., & Eicken, H. (2002). Sediment inclusions in Alaskan coastal sea ice: Spatial distribution, interannual variability, and entrainment requirements. *Arct. Antarct. Alp. Res.*, *34*(4), 465–476. doi: 10.1080/15230430.2002.12003518

Stroeve, J. C., & Notz, D.   (2018).   Changing state of Arctic sea ice across all seasons. *Environ. Res. Lett.*, *13*(10). doi: 10.1088/1748-9326/aade56

Stroeve, J. C., Serreze, M. C., Holland, M. M., Kay, J. E., Malanik, J., & Barrett, A. P.   (2012).   The Arctic's rapidly shrinking sea ice cover: A research synthesis. *Clim. Change*, *110*(3-4), 1005–1027. doi: 10.1007/s10584-011-0101-1

Sunda, W. G., & Huntsman, S. A.   (1994).   Photoreduction of manganese oxides in seawater. *Mar. Chem.*, *46*(1-2), 133–152. doi: 10.1016/0304-4203(94)90051-5

Tagliabue, A., Bowie, A. R., Boyd, P. W., Buck, K. N., Johnson, K. S., & Saito, M. A.   (2017).   The integral role of iron in ocean biogeochemistry.   *Nature*, *543*(7643), 51–59. doi: 10.1038/nature21058

The Pandas development team. (2020). Pandas-dev/pandas: Pandas. *Zenodo*, *21*, 1–9.

Thyng, K. M., Greene, C. A., Hetland, R. D., Zimmerle, H. M., & DiMarco, S. F. (2016).   True colors of oceanography: Guidelines for effective and accurate colormap selection. *Oceanogr.*, *29*(3), 9–13.

Tilmes, S., Lamarque, J. F., Emmons, L. K., Kinnison, D. E., Marsh, D., Garcia, R. R., . . . Blake, N.   (2016).   Representation of the Community Earth System Model (CESM1) CAM4-chem within the Chemistry-Climate Model Initiative (CCMI). *Geosci. Model Dev.*, *9*(5), 1853–1890. doi: 10.5194/gmd-9-1853-2016

Tovar-Sánchez, A., Duarte, C. M., Alonso, J. C., Lacorte, S., Tauler, R., & Galbán-Malagón, C.   (2010).   Impacts of metals and nutrients released from melting multiyear Arctic sea ice.   *J. Geophys. Res.*, *115*(C7), C07003.   doi: 10.1029/2009JC005685

Tucker, W. B., Gow, A. J., Meese, D. A., Bosworth, H. W., & Reimnitz, E.   (1999). Physical characteristics of summer sea ice across the Arctic Ocean. *J. Geophys. Res.-Ocean.*, *104*(C1), 1489–1504. doi: 10.1029/98jc02607

Van Hulten, M., Middag, R., Dutay, J.-C., De Baar, H., Roy-Barman, M., Gehlen, M., . . . Sterl, A. (2017). Manganese in the west Atlantic Ocean in the context of the first global ocean circulation model of manganese.   *Biogeosciences*, *14*, 1123–1152. doi: 10.5194/bg-14-1123-2017

Virtanen, P., Gommers, R., Oliphant, T. E., Haberland, M., Reddy, T., Courna-peau, D., . . . others   (2020).   Scipy 1.0: fundamental algorithms for scientific computing in python. *Nature methods*, *17*(3), 261–272.

1300   Wang, Q., Myers, P. G., Hu, X., & Bush, A. B. G.   (2012).   Flow constraints on

1301   pathways through the Canadian Arctic Archipelago.   *Atmos.-Ocean*, *50*(3),

1302   373–385. doi: 10.1080/07055900.2012.704348

1303   Wang, S., Bailey, D., Lindsay, K., Moore, J. K., & Holland, M. (2014). Impact of sea

1304   ice on the marine iron cycle and phytoplankton productivity.   *Biogeosciences*,

1305   *11*(17), 4713–4731. doi: 10.5194/bg-11-4713-2014

1306   Waskom, M., & the Seaborn development team.   (2020).   *Seaborn*. Zenodo.   doi: 10

1307   .5281/zenodo.592845

1308   Wedepohl, H. K.   (1995).   The composition of the continental crust.   *Geochem. Cos-*

1309   *mochim. Acta*, *59*(7), 1217–1232. doi: 10.1016/0016-7037(95)00038-2

1310   Yamamoto-Kawai, M., McLaughlin, F. A., Carmack, E. C., Nishino, S., Shimada,

1311   K., & Kurita, N.   (2009).   Surface freshening of the Canada Basin, 2003–2007:

1312   River runoff versus sea ice meltwater. *J. Geophys. Res.*, *114*(C1), C00A05. doi:

1313   10.1029/2008JC005000

1314   Yeats, P. A., & Westerlund, S. (1991). Trace metal distributions at an Arctic Ocean

1315   ice island. *Mar. Chem.*, *33*(3), 261–277. doi: 10.1016/0304-4203(91)90071-4

1316   Zalesak, S. T. (1979). Fully multidimensional flux-corrected transport algorithms for

1317   fluids. *J. Comput. Phys.*, *31*(3), 335–362. doi: 10.1016/0021-9991(79)90051-2